Computers and Electrical Engineering 120 (2024) 109733

Contents lists available at ScienceDirect

Computers and Electrical Engineering

journal homepage: www.elsevier.com/locate/compeleceng

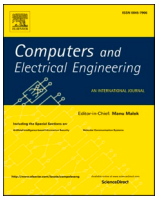

Reliability and security improvement of distribution system using optimal integration of WTDGs and SMESs considering DSTATCOM functionality based on an enhanced walrus optimization algorithm

Mohamed Khamies [a], Mohamed Hashem [b,*], Salah Kamel [c], Mohamed H. Hassan [d], Abdelfatah Ali [e]

[a] Department of Electrical Engineering, Faculty of Engineering, Sohag University, Sohag 82524, Egypt
[b] Holding Company for Water and Wastewater, Sohag, Egypt
[c] Electrical Engineering Department, Faculty of Engineering, Aswan University, Aswan 81542, Egypt
[d] Ministry of Electricity and Renewable Energy, Cairo, Egypt
[e] Electrical Engineering Department, South Valley University, 83523 Qena, Egypt

ARTICLE INFO

Keywords:
WTDGs and SMESs
DSTATCOM functionality
Reliability indices
Security index
Mixed load
Enhanced walrus optimization algorithm

ABSTRACT

This paper aims to improve the customer-oriented reliability indices (CORIs), load-oriented reliability indices (LORIs), and the security of the electric distribution system (EDS). This is achieved through the optimal placement and sizing of wind turbine distributed generators (WTDGs) and superconducting magnetic energy storages (SMESs), which incorporate DSTATCOM functionality. The LORIs include energy not supplied (ENS) and average energy not supplied (AENS), while the CORIs consist of the system average interruption frequency index (SAIFI), system average interruption duration index (SAIDI), average service unavailability index (ASUI), and customer average interruption duration index (CAIDI). The network security index (NSI), which assesses the risk of current flow in lines approaching critical levels, is also examined. A multi-objective function based on optimized weight factors is developed to simultaneously reduce NSI, ASUI, ENS, SAIDI, and SAIFI using an enhanced walrus optimization algorithm (EWaOA) along with sensitivity factors analysis. This optimizer is an improved form of the traditional Walrus Optimization Algorithm (WaOA), designed to balance exploration and exploitation stages better, thereby avoiding local optima and improving overall performance. The EWaOA algorithm's effectiveness is tested on seven benchmark functions and compared with the conventional WaOA and other recent algorithms. The paper also explores the discharge as well as charging real power in addition to initially SOC of SMESs. The proposed method is applied to the IEEE 33-bus EDS, considering a mixed time-varying voltage-dependent (TVVD) load model. The results indicate that the optimal integration of WTDGs and SMESs with DSTATCOM functionality significantly enhances the reliability and security of the tested EDS.

* Corresponding author.
E-mail address: mohamed.hashem575@eng.aun.edu.eg (M. Hashem).

https://doi.org/10.1016/j.compeleceng.2024.109733
Received 13 June 2024; Received in revised form 14 September 2024; Accepted 22 September 2024
Available online 1 October 2024

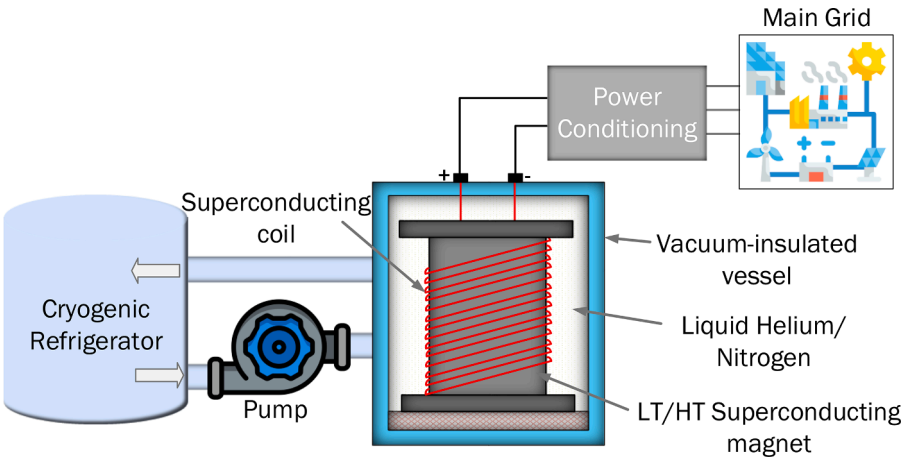

Fig. 1. Schematic diagram for the components of the SMES device [18].

1. Introduction

1.1. Motivation

Recently, the integration of wind turbine distributed generators (WTDGs) into electric distribution systems (EDSs) has gained significant attention among energy planners worldwide, offering the potential to reduce fossil fuel consumption and carbon emissions, while enhancing the technical performance of power networks in place of conventional energy sources. Without a doubt, WTDGs and photovoltaic (PV) systems are the most widely adopted renewable sources due to their adaptability and cost-effectiveness [1-3]. Renewable energy sources (RES) notably enhance the performance of EDSs, particularly through the Distribution Static Compensator (DSTATCOM) functionality of inverters interfacing these sources, which improves reliability, voltage profiles, power loss mitigation, power quality, and reduces the load on conventional Var sources [4-6].

However, the inherent unpredictability of factors such as wind speed, solar irradiance variations, and fluctuating load demands introduces substantial operational and practical challenges to EDS reliability, including power outages and security issues like line overloading [7-9]. Overcoming these challenges to achieve the desired outcomes is a formidable task, underscoring a pivotal issue in both the planning and operational phases of integrating renewable sources and storage devices, necessitating careful consideration.

Despite the various benefits of radial EDSs, these systems, with their radial structure, have a restriction on low reliability, which has the highest impact on the unavailability of supply and forced outages for customers. Also, the security indicator concerns the excessive loading of network branches above their nominal transfer capacity [10,11].

Nowadays, superconducting magnetic energy storage (SMES) is one of the most popular and significant kinds of energy storage units because of its great power (0.1–10 MW), long lifespan, high efficiency of 98 %, rapid response time and unlimited charging and discharging cycles [12,13]. As a result, the SMES device is thought to be able to meet the predictable peak load in addition to resolving different EDS concerns, such as improving both voltage-dip, transient stability, and power quality. However, the use of liquid nitrogen for efficient cooling in a high-temperature superconducting coil (SC) can drastically reduce the excessive cost and the mechanical stress of the SMES [14-16].

The SMES device is considered a significant SC that stores electrical energy through a magnetic field generated by a DC flow, exhibiting zero losses at cryogenic temperatures. Depending on the load profile, the SMES device can either generate or consume active and reactive powers. Fig. 1 depicts a schematic diagram of the SMES device, comprising a superconducting coil, a nitrogen cryogenic refrigerator for maintaining superconducting conditions, and a power conditioning system (PCS) connected to the external grid [17, 18].

1.2. Literature review

A variety of research techniques have been addressed for enhancing the reliability of the EDSs, involving the inclusion of renewable energy resources (RESs), the integration of ESSs, network reconfiguration, and capacitor banks. The impact of electric vehicles on EDSs has been investigated using a probabilistic reliability-based assessment approach. The reliability metrics utilized include the average service availability indicator (ASAI), the SAIDI, the ENS, and the SAIFI [19]. Optimally allocated battery ESSs were demonstrated for improving the reliability of the EDS according to ENS and ESSs life cycle cost based on the grey wolf algorithm [20] and teaching-learning-based algorithm [21]. Optimal sizing and scheduling of battery system for improving the reliability and performance of EDSs integrated with uncertain solar sources have been studied [22]. Optimal inclusion of battery storage along with RESs simultaneously in an EDS for minimizing electrical power loss and enhancing ENS, ASAI, AENS, SAIDI, and SAIFI in [23], as well as reducing both ENS, voltage dip, power losses, and load cost in the EDS [24]. The goals regarding ENS and minimizing power losses are

rooted in the sine-cosine Optimizer [25]. Additionally, the refined and bolstered hybrid algorithms [26] was used for optimizing the placement and capacity ratings of RESs. Exploring ENS as a reliability benchmark, our study delved into enhancing stability, improving voltage profiles, and minimizing power losses [27] through a coordinated allocation of RESs alongside network reconfiguration.

The work discusses a reconfiguration-based approach [28] aimed at bolstering reliability indicators such as SAIDI, ENS, and SAIFI, while simultaneously reducing power losses. This is achieved through a customized adaptation of the genetic algorithm. The network's reconfiguration along with ESSs capability was applied in order to assess the short-term reliability indicators, comprising the risk of ENS and customer minute loss [29]. ENS enhancement as well as maximization of cost-saving based on the SCA was studied using the optimal inclusion of RESs and capacitors [30] and the optimal allocation of capacitors [31]. A suggested approach [32] for the optimal integration of SMESs and WTDGs within an EDS aims to enhance reliability indicators and the line loading index. This method employs a hybrid scheme combining equilibrium optimization with sensitivity factors, though it does not account for uncertainties in the system's components.

The DSTATCOM capability of renewable sources-interfacing inverters has been employed in literature for diverse applications. For instance, in [33-35], the authors enabled the DSTATCOM functionality of connected inverters to maximize the hosting capacity of RES in EDSs. Moreover, in [36], optimal allocation of inverter-based PVs in IEEE 33-bus EDS equipped with their inherent DSTATCOM capability for improving ENS, AENS, SAIFI, SAIDI, CAIDI, ASUI, and NSI using particle swarm algorithm with the consideration of uncertainty in both PV power generation and the load profile.

Furthermore, the survey [37-40] delves into enhancing the network's security, particularly by minimizing line loading. In the IEEE 33-bus EDN, this involved optimizing the allocation of different ESSs to minimize line loading and various objective functions (OFs). Specifically, in [37], active power delivery was optimized, while [38,39] explored optimal ESS allocation considering both active and reactive power delivery. Moreover, [40] demonstrates the effective integration of RESs and capacitors to mitigate line loading and various OFs in a rural EDS, accounting for the stochastic uncertainty associated with RESs. Moreover, the reliability and security of the IEEE 33-bus EDN with constant load are enhanced by assigning the optimal planning of uncertain multiple WTGs along with optimized plug-in electric vehicles (PEVs) with controlled and uncontrolled charging patterns using a bi-level particle swarm algorithm with the consideration of the impacts of the annual load growth on the EDN's reliability and security. The DSTATCOM functionality of the WTDG interfacing inverter and the ASUI function are not considered. The weighting factors of the investigated objective functions are considered as constant values [41].

1.3. Research gaps

According to the aforementioned studies presented in Section 1.2, most research studies addressed many methods in the area of enhancing some of individual reliability indices as problem formulation. Besides, a minimization of weighted-sum multi-objective function accommodating the LORIs, CORIs, and the network security index using WTDGs and SMESs incorporating DSTATCOM functionality based on an enhanced walrus optimization algorithm (EWaOA) along with sensitivity factors analysis has not been investigated before. Also, the mixed TVVD load model, protection device installation, and feeder failure rate model have a less attention of the researchers. Based on these gaps, one may ask whether the optimal integration of WTDGs and SMESs considering DSTATCOM Functionality can enhance the EDS's reliability and security. Additionally, the proposed EWaOA algorithm can be able to solve the investigated problem and find an optimal solution with a lesser computational time.

1.4. Research novelties

The main contributions of this study could be summarized as follows:

- ✓ Developing an optimized approach for siting and rating WTDGs and SMESs, incorporating their DSTATCOM functionality. This aims to bolster the reliability and security of the EDS by concurrently minimizing ENS, SAIFI, SAIDI, ASUI, and NSI as Multi-Objective Functions (MOF) using optimized weight factors.
- ✓ Utilizing sensitivity analysis to identify optimal buses for integrating WTDGs and SMESs.
- ✓ Enhancing the performance of the traditional Walrus Optimization Algorithm (WaOA) by proposing an improved version, named EWaOA.
- ✓ Investigating the optimal SMESs discharge as well as charging real powers, in addition to initially SOC.
- ✓ Examining the impact of protection device installation and the feeder failure rate (FFR) on the EDS's reliability values.
- ✓ Evaluating the effectiveness of the proposed method by applying a mixed TVVD load model on the IEEE 33-bus EDS.

1.5. Research organization

The main structure of this research unfolds as follows: Section 2 lays out the models for Load, WTDG, and SMES. In Section 3, the paper delves into problem identification and its associated constraints concerning the reliability and security enhancement of the EDS using WTDGs and SMESs. Meanwhile, Section 4 introduces both the original and enhanced Walrus Optimization Algorithm. Section 5 offers an in-depth evaluation of the proposed EWaOA through benchmark functions test as well as its application for enhancing the reliability and security of the IEEE 33-bus System. Lastly, Section 6 encapsulates the conclusions drawn from this study.

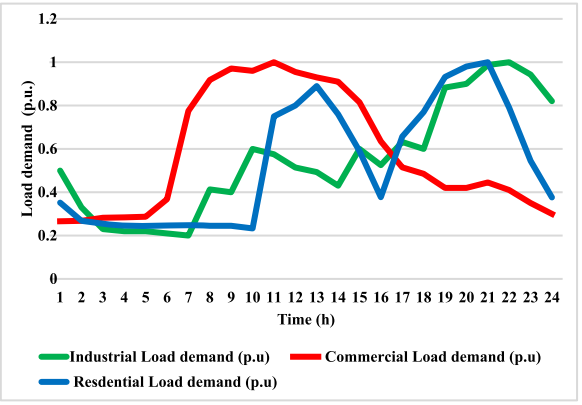

Fig. 2. Normalized different load demand over the whole day [43].

2. Load-demand, WTDG, and SMES models

2.1. Load-demand model

Different load demand models over the whole day are investigated in this present study involving residential, industrial, and commercial load models at the highest possible level of 1 p.u. Furthermore, Fig. 2 shows the normalized different load demand over the whole day. The hourly active load power $P_j(t)$ and reactive load power $Q_j(t)$ as a function of voltage exponents at load point j for each load model are presented as follows:

$$P_j(t) = P_{oj}(t) \times V_j^{\rho}(t) \tag{1}$$

$$Q_j(t) = Q_{oj}(t) \times V_j^{\sigma}(t) \tag{2}$$

where V_j represents the voltage at load node j, Q_{oj} and P_{oj} denote the reactive and real load power for the rated voltage at node j, accordingly., as well as the $\boldsymbol{\sigma}$ and ρ represent reactive and real load voltage exponents, respectively, which their values are given in [42].

2.2. WTDG model

The output power produced by the WTDG ($P^{WTDG,\text{rated}}$) during wind speed v_w can be determined as follows:

$$P_{WTDG} = \begin{cases} 0 & \text{if} \quad v_w \langle v_{ci} \text{ and } v_w \rangle v_{co} \\ P^{WTDG,\ \text{rated}} \left(\dfrac{v_w - v_{ci}}{v_{w,r} - v_{ci}} \right) & \text{if} \quad (v_{ci} \le v_w \le v_{w,r}) \\ P^{WTDG,\ \text{rated}} & \text{if} \quad (v_{w,r} < v_w \le v_{co}) \end{cases} \tag{3}$$

where v_{co}, $v_{w,r}$, and v_{ci} are cut-out wind speed, rated wind speed, and cut-in wind speed of the WTDG, respectively; $P^{WTDG,\text{rated}}$ represents the WTDG's rated power. The WTDG parameters as well as the wind speed profile used in this present study are presented in [44,45].

2.3. Charging and discharging modes of the SMES

In the charging state of the SMES, it works as a load-demand, which can store the additional produced power of the WTDGs when the load power P_L is lesser than WTDGs power.

$$P_S(t) = \max\{ -|\Delta \mathrm{P(t)}|, \frac{(E_S(t-1) - E_{S,max})}{\Delta \mathrm{t}\ \eta_C}, -P_{S,rated} \} \tag{4}$$

$$SOC_S(t) = \min\left\{ \left(SOC_S(t-1) - \frac{P_{S,C}(t) \Delta \mathrm{t}\ \eta_C}{E_{S,rated}} \right), SOC_{S,max} \right\} \tag{5}$$

During the discharging mode of the SMES, the device operates as a generator, supplying power to meet the load whenever the power from the WTDG falls below the load requirement.

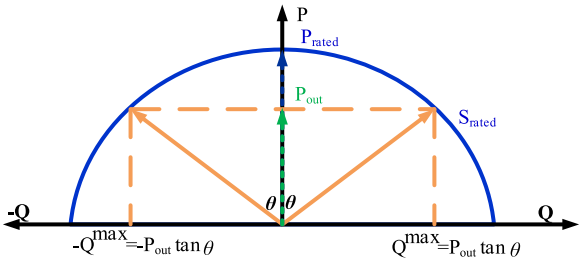

Fig. 3. Reactive power capability of the interfacing inverters.

$$P_S(t) = \max\{|\Delta P(t)|, \frac{(E_S(t-1) - E_{S,min})\eta_D}{\Delta t}, P_{S,rated}\} \tag{6}$$

$$SOC_S(t) = \max\left\{\left(SOC_S(t-1) - \frac{P_{S,D}(t)\Delta t}{\eta_D * E_{S,rated}}\right), SOC_{S,min}\right\} \tag{7}$$

where $P_S(t)$ is the power exchange in the SMES device during each hour, with positive negative, and zero estimates through the discharging state,charging state, and idle state of the SMES device, respectively; $\Delta P(t)$ is the difference between WTDGs and load powers; η_C and η_D are charging and discharging efficiencies, respectively; $P_{S,rated}$ is the rated power of SMES;$SOC_S(t)$ represents the SMES's SOC during each hour, indicating the energy stored within it;$SOC_{S,min}$ and $SOC_{S,max}$ defines the lower and upper SOC boundaries of the SMES, respectively; Δt signifies the time interval. The SMES's initial SOC (SOC_{init}) is also optimized [46-48].

2.4. DSTATCOM functionality of WTDG and SMES interfacing inverters

To achieve voltage regulation within EDS, a proactive approach involves optimizing the functionality of interfacing inverters. Emphasized within the IEEE 1547 standard, this approach underscores the significance of effectively managing reactive power capabilities. The graphical representation in Fig. 3 explains the operational boundaries of these inverters, portrayed as a semicircle. Notably, the inverter's capacity is delineated by its rated capacity (S_{rated}) with P_{out} illustrating active power outputs of WTDG/SMES and Q^{max}denoting maximum reactive power capacity. When operating at peak active power injection levels (i.e., $P_{rated} = S_{rated}$), the injected/absorbed reactive power will be zero. Hence, the inverter's reactive power dynamics are contingent upon both its rated capacity and the system's output power. Consequently, adherence to inverter capacity constraints necessitates rigorous computation of reactive power thresholds for WTDGs and SMESs inverters, as follows.

$$\begin{cases} Q_t^{WTDG,max} = \sqrt{\left(S^{WTDG,\ \text{rated}}\right)^2 - \left(P_t^{WTDG}\right)^2} \\ Q_t^{WTDG,\ \min} = -\sqrt{\left(S^{WTDG,\ \text{rated}}\right)^2 - \left(P_t^{WTDG}\right)^2} \end{cases} \tag{8}$$

$$\begin{cases} Q_t^{S,max} = \sqrt{\left(S^{S,\ \text{rated}}\right)^2 - \left(P_t^{S}\right)^2} \\ Q_t^{S,\ \min} = -\sqrt{\left(S^{S,\ \text{rated}}\right)^2 - \left(P_t^{S}\right)^2} \end{cases} \tag{9}$$

where $S^{WTDG,\text{rated}}$and $S^{S,\text{rated}}$represent the rated capacity of the interfacing inverters of WTDG and SMES, respectively; $P_t^{WTDG}$and $P_t^S$are the output powers of the WTDG and SMES, respectively; the superscripts *min* and *max* indicate the minimum and maximum values, respectively.

3. Problem identification

This section presents the identification of various OFs to improve the studied EDS's reliability and security. To achieve this objective, the work addresses the simultaneous optimization of optimal sites and ratings for WTDGs and SMESs, both with and without their DSTATCOM functionality. This optimization aims to enhance the LORIs, CORIs, and security index of the EDS. The locations and ratings of DG units are typically selected based on an objective function designed to enhance the reliability and security of the distribution system. This objective function guides the selection process.

The proposed EWaOA is employed to determine the optimal locations and ratings of DG units. The algorithm iteratively searches for the best combination of locations and ratings that satisfy the defined objective while adhering to system constraints. A set of candidate buses is pre-determined using sensitivity analysis where DG units can potentially be placed. The algorithm evaluates different combinations of these candidate buses to identify the optimal locations that contribute to the overall system performance improvement.

On the other hand, the ratings of the DG units are determined by considering the maximum allowable capacity for each unit and the impact of different capacities on the system. The EWaOA adapts the DG ratings during the optimization process, adjusting them to

ensure they provide the best possible performance in terms of the objective function. Then, the final locations and ratings are those that yield the most favorable outcomes according to the objective function while satisfying all system constraints. The EWaOA's ability to handle complex, non-linear optimization problems ensures that the selected DG placements and sizes are both efficient and effective.

In this current study, the following objective functions (OFs) can be written as follows:

$$Obj.Funct._{\vartheta} = \min\left\{\omega_1 f_{obj1} + \omega_2 f_{obj2} + \omega_3 f_{obj3} + \omega_4 f_{obj4} + \omega_5 f_{obj5}\right\}, \tag{10}$$

where:

$$\omega_1 + \omega_2 + \omega_3 + \omega_4 + \omega_5 = 1, \tag{11}$$

where ϑ is the decision variables vector which comprises the optimal sizes and locations of the WTDGs and SMESs along with hourly optimal powers of charging and discharging of the SMESs; ω_1,ω_2,ω_3,ω_4 and ω_5 are the optimal weighting factors. It is worth to mention that the sensitivity analysis is used to obtain the candidate sites of the WTDGs and SMESs [32].

The several OFs can be mathematically expressed as follows [49,50]:

$$f_{obj1} = ENS = \sum_{\mathscr{P}=1}^{N_{\mathscr{P}}} L_{\mathscr{P}}^{\text{man}} U_{\mathscr{P}}. \tag{12}$$

This OF denotes the represents the cumulative energy shortfall experienced by customers due to line failures, measured in MWh per year. $\mathscr{P}$ denotes the load point; $N_{\mathscr{P}}$ is the number of load nodes; $L_{\mathscr{P}}^{\text{man}}$ signifies the annual average load demand at load node $\mathscr{P}$; $U_{\mathscr{P}}$ represents the total annual hours of power supply unavailability (measured in hours per year) at load node $\mathscr{P}$.

Upon computing the ENS value, the average energy not supplied (AENS) can be determined. AENS is defined as the ratio of ENS value to the customers' number ($\text{NC}_{\mathscr{P}}$) at load node $\mathscr{P}$ over the course of the year, measured in kWh per customer per year. This can be calculated using the formula:

$$AENS = \frac{ENS * 1000}{\sum_{\mathscr{P}=1}^{N_{\mathscr{P}}} \text{NC}_{\mathscr{P}}} \tag{13}$$

The second objective function can be calculated by,

$$f_{obj2} = SAIFI = \frac{\sum_{\mathscr{P}=1}^{N_{\mathscr{P}}} \lambda_{\mathscr{P}} \text{NC}_{\mathscr{P}}}{\sum_{\mathscr{P}=1}^{N_{\mathscr{P}}} \text{NC}_{\mathscr{P}}}. \tag{14}$$

This OF illustrates the average frequency of service interruptions encountered by a customer (interruptions /customer/year). $\lambda_{\mathscr{P}}$ is the average failure, which is one of the investigated reliability indices and can be evaluated by [51],

$$\lambda_{\mathscr{P}} = \sum_{i=1}^{N_{out}} \lambda_i, \tag{15}$$

In this equation, λ_i denotes the failure rate of the i^{th} component; N_{out} indicates the total number of outages impacting load node $\mathscr{P}$. The linear correlation assesses the failure rate λ_i^{Lin} t concerning the compensation percentage when the current flowing in the branch is not entirely compensated. This relationship is established as follows [52]:

$$\lambda_i^{Lin} = \frac{\lambda_i^{init} - \lambda_i^{best}}{\left|I_i^{old}\right|} \times \left|I_i^{new}\right| + \lambda_i^{best} \tag{16}$$

In this context, λ_i^{best} and λ_i^{init} represent the best and initial failure rates, respectively. $|I_i^{new}|$ and $|I_i^{old}|$ denote the magnitude of current flowing in the i^{th} feeder after and before the inclusion of WTDGs and SMESs.

The third OF describes the average outage time experienced by a customer per year, measured in hours per customer per year. It can be formulated as follows:

$$f_{obj3} = SAIDI = \frac{\sum_{\mathscr{P}=1}^{N_{\mathscr{P}}} U_{\mathscr{P}} \text{NC}_{\mathscr{P}}}{\sum_{\mathscr{P}=1}^{N_{\mathscr{P}}} \text{NC}_{\mathscr{P}}}, \tag{17}$$

in which $U_{\mathscr{P}}$ is the annual outage time and can be calculated by,

$$U_{\mathscr{P}} = \sum_{i=1}^{N_{out}} \lambda_i r_i, \tag{18}$$

where r_i represents the repair time of the i^{th} component in hours.

Upon calculating the SAIDI value, the fourth OF depicts the ASUI, which represents the time when power, as needed by system consumers, was unattainable for all the 8760 h in a year. It can be calculated as follows:

$$f_{obj4} = ASUI = \frac{\sum_{\mathscr{P}=1}^{N_{\mathscr{P}}} U_{\mathscr{P}} \mathrm{NC}_{\mathscr{P}}}{8760 * \sum_{\mathscr{P}=1}^{N_{\mathscr{P}}} \mathrm{NC}_{\mathscr{P}}} \tag{19}$$

The last OF is the network security index (*NSI*), which can be computed by,

$$f_{obj5} = NSI = \frac{\sum_{\ell=1}^{N_\ell} \frac{I_\ell}{I_\ell^{\max}}}{N_\ell}, \tag{20}$$

where I_ℓ and $I_\ell^{\max}$ are the line current and its maximum value, respectively; N_ℓ represents the total number of lines. This function illustrates that if a line current rises to its maximum value, the respected line will be overloaded. Minimizing this OF will lead to reducing the outages of power branches, which improves the security of the studied system.

3.1. Constraints of the problem

The following problem constraints are needed for solving the investigated optimization problem including:

3.1.1. Equality constraints

$$P_{Sub}(t) + \sum_{p=1}^{n_p} P_{WTDG,p}(t) + \sum_{p=1}^{n_p} P_{S,p}(t) = \sum_{\ell=1}^{n_\ell} P_{loss,\ell}(t) + \sum_{p=1}^{n_p} P_{L,p}(t) \tag{21}$$

$$Q_{Sub}(t) = \sum_{\ell=1}^{n_\ell} Q_{loss,\ell}(t) + \sum_{p=1}^{n_p} Q_{L,p}(t) \tag{22}$$

where $P_{Sub}(t)$ and $Q_{Sub}(t)$ presents the substation's real and reactive powers during each hour. The active and reactive powers of load at node p during each hour are denoted by $P_{L,p}(t)$ and $Q_{L,p}(t)$, respectively. Additionally, $P_{loss,\ell}(t)$ and $Q_{loss,\ell}(t)$ represent the real and reactive power losses of line ℓ during each hour.

3.1.2. Inequality constraints

It is worth mentioning that to handle the inequality constraints, only agents that satisfy the constraints are retained for the next generation. This ensures that the optimization process adheres strictly to the defined boundaries and maintains feasible solutions throughout the iterations.

The current flow I_ℓ through branches during each hour must be saved within permissible limits as follows:

$$I_\ell(t) \le I_\ell^{max} \tag{23}$$

The voltage magnitude at each load point during every hour must adhere to predetermined permissible limits, defined as follows:

$$V_{min} \le V_p(t) \le V_{max} \tag{24}$$

where V_{min} and V_{max} represent the lower and upper voltage values, respectively, where the lower value equal to 0.95 p.u. and the upper value equal to 1.05 p.u.

The rated power of each WTDG should be considered in this limit:

$$\sum_{p=1}^{n_p} P_{w,r,p} \le P_{WTDG,max} \tag{25}$$

where the $P_{WT,max}$ are equal to the peak load value of each type.

The limits related to the rate of power $P_{S,rated}$ and energy storage capacity $E_{S,rated}$ of the SMES can be presented in Eq. (26) and Eq. (27), respectively,

$$P_{S,rated,min} \le P_{S,rated} \le P_{S,rated,max} \tag{26}$$

where $P_{S,rated,\ min}$ and $P_{S,rated,\ max}$ shows the minimum and maximum bounds of the rated power of the SMES, respectively.

$$E_{S,rated,min} \le E_{S,rated} \le E_{S,rated,max} \tag{27}$$

where $E_{S,rated,\ min}$ and $E_{S,rated,\ max}$ represent the min and the max constraints of the sored energy of the SMES, respectively.

$$-P_{S,rated} \le P_S(t) \le +P_{S,rated} \tag{28}$$

Here, the negative and positive polarities of $P_{S,rated}$ shows the SMES can work in the charging and discharging states.

$$SOC_{S,min} \le SOC_S(t) \le SOC_{S,max} \tag{29}$$

where $SOC_{S,max}$ and $SOC_{S,min}$ are taken as 0.9 and 0.1, as investigated before [32].

Ensuring seamless operation for consecutive days, the SMES's final SOC ($SOC_S(T)$) at the conclusion of entire day time should remain primed for continuous utilization on the following day time. This is achieved by setting it equivalent to the initially SOC ($SOC_S(0)$) as outlined in [32]:

$$SOC_S(T) = SOC_S(0) \tag{30}$$

The injected and absorbed reactive power of the connected inverters of WTDG and SMES must remain within specified thresholds, a condition that can be mathematically expressed as:

$$Q_t^{WTDG,min} \le Q_t^{WTDG} \le Q_t^{WTDG,max} \tag{31}$$

$$Q_t^{S,min} \le Q_t^{S} \le Q_t^{S,max} \tag{32}$$

where $Q_t^{WTDG}$and Q_t^S are the reactive power delivered and consumed by WTDG and SMES interfacing inverters, respectively.

4. Optimization technique

4.1. The original algorithm

The Walrus Optimization Algorithm (WaOA), which mimics walrus behavior during migration, was inspired by natural phenomena [52]. These creatures inhabit cold climates, usually close to the North Pole. In a herd, the male that has the largest muscles and the longest tusks is regarded as the dominant member who guides the group. When the ice begins to crack and melt during the annual onset of summer, Walruses tend to migrate to stony beaches or outcrops. However, this journey poses risks due to their natural predators, including the polar bear and the killer whale, also known as orca. The algorithm simulates the movements of three majestic walruses, reflecting their behaviors.

- Leading the group to eat: at this point, the dominant walrus, who is the best individual, is tracked to direct the other individuals into regions of potential. This leads to significant shifts in the locations of the individuals. This stage maximizes the algorithm's capacity for global search and exploration, enhancing its ability to navigate through a wide range of possibilities.
- Herd migration: This stage significantly alters people's places yet again. The locations of the people are thought to be likely migratory destinations. When a random position is chosen, the other participants advance toward it. To evade premature convergence and getting trapped in local optima, the population update at this stage ensures that it doesn't rely solely on a single member, even if that member currently holds the best position.
- Predator battle or flee: in this stage, individual walrus positions are somewhat altered as they confront their predators in constrained areas surrounding their positions. Better convergence is achieved and the algorithm's capacity for local search and exploitation is enhanced.

Mathematically, the process can be represented as follows:

i **Initialization**: the plotting of the population as:

$$X = \left[X_{m,n}\right] = \begin{bmatrix} X_{1,1} & \cdots & X_{m,1} \\ \vdots & \ddots & \vdots \\ X_{1,n} & \cdots & X_{m,n} \end{bmatrix} \tag{33}$$

$$F = \begin{bmatrix} F_1 \\ \vdots \\ F_N \end{bmatrix} = \begin{bmatrix} F(X_1) \\ \vdots \\ F(X_N) \end{bmatrix} \tag{34}$$

where n represents the people number, m denotes the decisions' number, F signify the desired objective function, and X is the WaOA population.

i **Feeding strategy:**

The person with the tallest tusks, or the best solution, leads the other individuals to the best feeding place in this step. The strongest person comes up with the best answer. The dominant (strongest) walrus leads the update of the positions, which can be mathematically represented as follows:

$$X_{i,j}^{L1} = X_{i,j} + rnd_{i,j}.\left(SW_j - I_{i,j}.X_{i,j}\right) \tag{35}$$

$$X_i = X_i^{L1}, F_i^{L1} < F_i; else : X_i = X_i \tag{36}$$

where X_i^{L1} represents the updated location discovered for walrus i based on the feeding tactic; $X_{i,j}^{L1}$ denotes its j^{th} dimension; F_i^{L1} indicates its objective function value; $rnd_{i,j}$ are random numbers drawn from the interval [0, 1]; SW represents the best candidate solution, identified as the strongest walrus; $I_{i,j}$ are randomly selected integers from either 1 or 2. These integers contribute to enhancing the algorithm's exploration capability.

i **Migration:**

This step simulates the walrus's migration to stony areas or outcrops, where each individual randomly chooses the position of another individual in a different section of the search space. The present location is replaced if the newly suggested site yields superior results for the objective function. This has the following mathematical expression:

$$X_{i,j}^{L2} = X_{i,j} + rnd_{i,j}.\left(X_{Kj} - I_{i,j}.X_{i,j}\right), F_K < F_i; else : X_{i,j}^{L2} = X_{i,j} + rnd_{i,j}.\left(X_{i,j} - X_{k,j}\right) \tag{37}$$

$$X_i = X_i^{L2}, F_i^{L2} < F_i; else : X_i = X_i \tag{38}$$

where X_i^{L2} signifies the recently generated location for the i^{th} walrus during the second stage, $X_{i,j}^{L2}$ represents its j^{th} dimension, F_i^{L2} denotes its fitness functional output. X_k, where k ∈ {1, 2, …, N} and k ≠ i, indicates the position of the chosen seahorse to which the i^{th} seahorse migrates. X_{Kj}represents the j^{th} dimension of the selected seahorse, and F_K represents its fitness functional output.

i **Marauder escape or competition:**

They battle and flee from their predators in the vicinity of their present sites because of the likelihood of being attacked. Imitating this kind of behavior enhances the effectiveness of the local search algorithm. This has the following mathematical expression:

$$X_{i,j}^{L3} = X_{i,j} + (LL_{lcl,j}^t + \left(UL_{lcl,j}^t - rnd.LL_{lcl,j}^t\right) \tag{39}$$

$$Local\ limits : LL_{lcl,j}^t = \frac{LL_j}{t}; UL_{lcl,j}^t = \frac{UL_j}{t} \tag{40}$$

$$X_i = X_i^{L3}, F_i^{L3} < F_i; else : X_i = X_i \tag{41}$$

where X_i^{L3} refers to the newly created location for the i^{th} walrus according to the 3_{rd} phase, $X_{i,j}^{L3}$ represents its j_{th} dimension, F_i^{L3} denotes its fitness functional output, t indicates the iteration curve, LLj, and ULj are the lowest and maximum limits of the j_{th} variable, respectively, $LL_{lcl,j}^t$ as well as $UL_{lcl,j}^t$ are local minimum and local maximum limits permissible for the j_{th} variable, respectively, to imitate local searches within the proximity of the nominee solutions.

4.2. The improved EWAOA technique

The "High and Low Velocity Ratios" method denotes an enhancement proposed based on the Marine Predator Algorithm (MPA) [53]. This method has been applied to improve several techniques and helped to solve many optimization problems such as the parameters of the controller combine proportional-integral-derivative (PID) and fractional order control methods using Enhanced Runge Kutta Optimizer [54] and optimal size and location of several FACTS devices to achieve minimizing fuel costs and minimizing power losses using Enhanced Tuna Swarm Optimization [55]. This enhancement addresses the challenge of potential entrapment at a local minimum in finding the optimal solution. The high-velocity ratio stage constitutes the initial phase of this method. The mathematical model for this stage is defined by Eqs. (42.1 to 42.3).

$$t < \frac{1}{3}T_{max} \tag{42.1}$$

$$S = \overrightarrow{R_B} \otimes \left(E - \overrightarrow{R_B} \otimes x_i(t)\right) \tag{42.2}$$

$$x_i(t+1) = x_i(t) + P.\overrightarrow{R_B} \otimes S \tag{42.3}$$

In these expressions, $\overrightarrow{R_B}$ represents a vector of random integers drawn from a normal distribution, simulating Brownian motion, while ⊗ signifies element-wise multiplication. The updated location is obtained by multiplying $\overrightarrow{R_B}$ with the previous position, using P

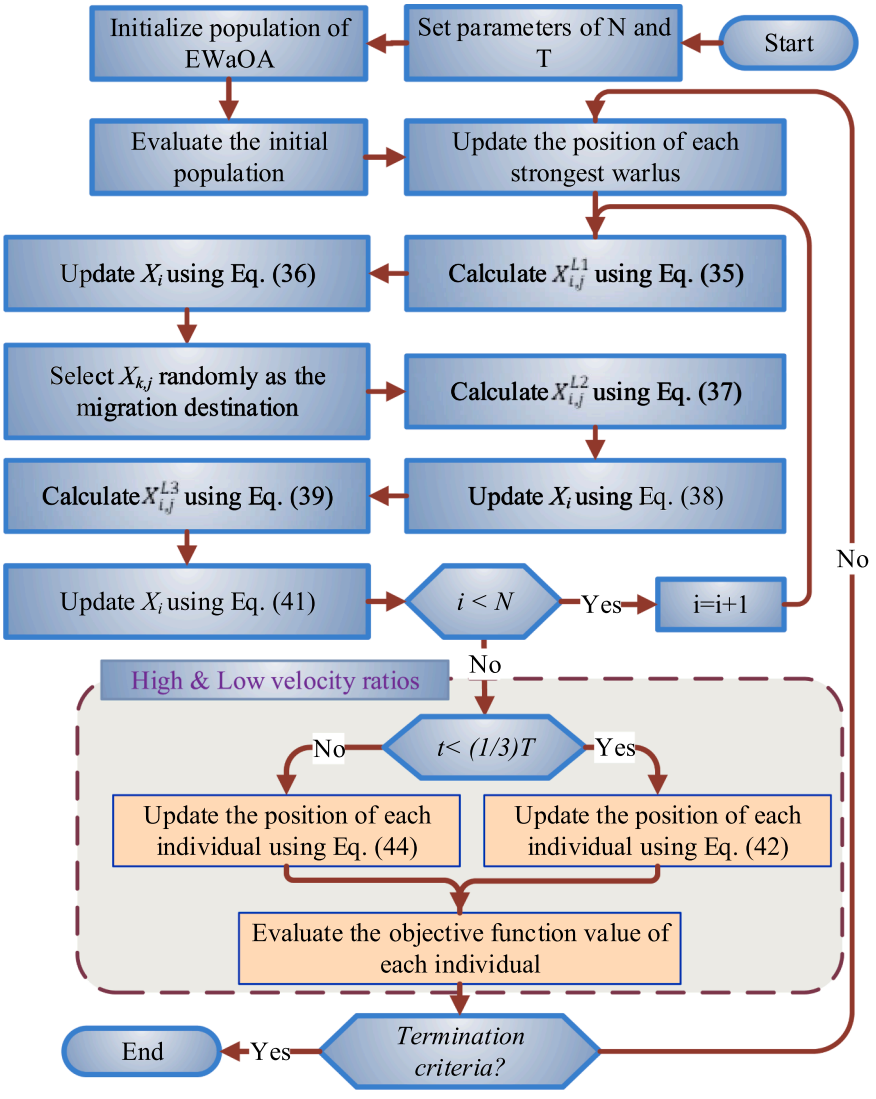

Fig. 4. Flowchart of proposed EWaOA algorithm.

Table 1
The statistical outcomes from the evaluation of 7 benchmark functions employing the EWaOA algorithm alongside other contemporary approaches.

Function		EWaOA	WaOA	JS	INFO	TSO	ARO
F1	Best	1.4E-307	1.2E-116	6.48E-15	4.44E-49	4.6E-118	1.59E-26
	Average	7.1E-280	4.2E-113	7.73E-12	1.84E-43	1.07E-94	1.07E-21
	Median	9.1E-292	7.8E-114	5.7E-13	9.67E-46	5.3E-106	4.68E-23
	Worst	1.3E-278	2.6E-112	1.22E-10	2.45E-42	2.15E-93	7.08E-21
	std	0	6.8E-113	2.71E-11	5.79E-43	4.8E-94	2.18E-21
	Rank	1	2	6	4	3	5
F2	Best	6.3E-153	5.86E-60	1.13E-07	1.08E-24	2.98E-58	1.34E-14
	Average	9.8E-146	1.07E-57	3.31E-06	1.83E-22	1.66E-50	1.15E-12
	Median	1.1E-147	3.97E-58	1.5E-06	1.11E-23	2.01E-52	1.22E-13
	Worst	8E-145	9.08E-57	1.67E-05	3.2E-21	2.41E-49	1.78E-11
	std	2.1E-145	2.08E-57	4.46E-06	7.11E-22	5.44E-50	3.94E-12
	Rank	1	2	6	4	3	5
F3	Best	1.3E-295	9.94E-89	0.043236	1.16E-39	3.4E-113	4.28E-21
	Average	1.7E-270	1.94E-82	37.7777	1.27E-32	1.48E-89	5.08E-15
	Median	1.5E-274	5.51E-86	2.63887	4.71E-35	9.2E-100	6.99E-17
	Worst	2.1E-269	3.72E-81	289.5644	1.65E-31	2.79E-88	6.41E-14
	std	0	8.3E-82	76.37593	3.71E-32	6.24E-89	1.51E-14
	Rank	1	3	6	4	2	5
F4	Best	1.4E-145	2.29E-56	1.66E-08	1.21E-22	4.03E-60	8.35E-13
	Average	2.2E-137	2.76E-54	2.28E-07	8.95E-19	8.06E-49	2.6E-09
	Median	3E-141	5.56E-55	1.66E-07	1.88E-20	1.61E-50	7.79E-10
	Worst	4.1E-136	2.11E-53	7.36E-07	1.5E-17	8.05E-48	2.28E-08
	std	9.2E-137	5.46E-54	1.78E-07	3.34E-18	1.89E-48	5.09E-09
	Rank	1	2	6	4	3	5
F5	Best	0.030462	0.045605	0.042193	23.12486	3.3E-05	0.048127
	Average	0.09287	0.148116	0.654502	24.43097	2.932789	2.57084
	Median	0.085141	0.156112	0.458008	24.41788	0.100044	1.069097
	Worst	0.205322	0.346533	2.763539	25.78378	26.85013	16.26736
	std	0.04706	0.082098	0.735235	0.620893	8.100797	3.783419
	Rank	1	2	3	6	5	4
F6	Best	2.43E-08	3.89E-06	9.87E-07	1.16E-06	5.72E-06	0.009568
	Average	5.37E-08	9.76E-05	2.02E-05	1.47E-05	0.003695	0.044563
	Median	4.9E-08	0.000113	1.68E-05	8.52E-06	0.00104	0.039666
	Worst	1.11E-07	0.000154	6.11E-05	3.81E-05	0.018609	0.098375
	std	2.35E-08	3.97E-05	1.86E-05	1.31E-05	0.00494	0.026373
	Rank	1	4	3	2	5	6
F7	Best	1.02E-05	5.73E-06	0.000288	0.000201	2.22E-05	3.22E-05
	Average	8.66E-05	8.53E-05	0.001159	0.00178	0.000684	0.001407
	Median	7.07E-05	7.24E-05	0.000994	0.00135	0.00065	0.00115
	Worst	0.00021	0.000289	0.00267	0.005593	0.002054	0.003564
	std	6.02E-05	7.12E-05	0.000648	0.001428	0.000585	0.001071
	Rank	2	1	4	6	3	5
Average Rank		1.142857	2.285714	4.857143	4.285714	3.428571	5
Final ranking		1	2	5	4	3	6

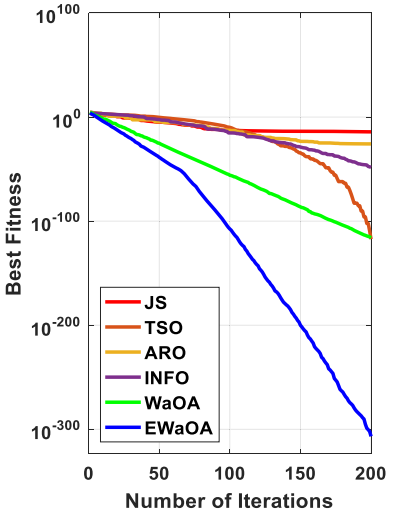

F1

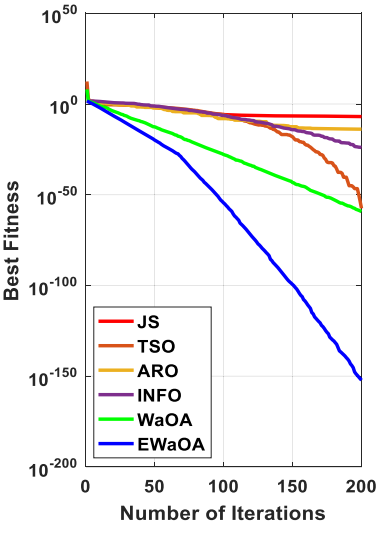

F2

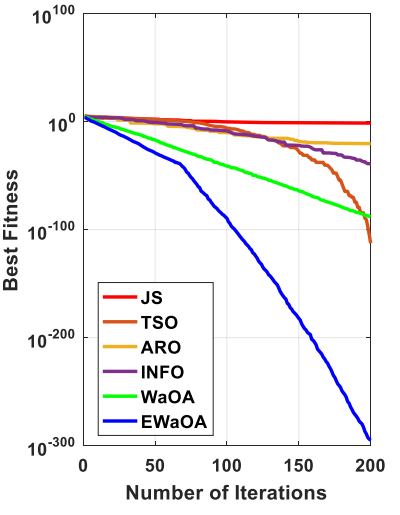

F3

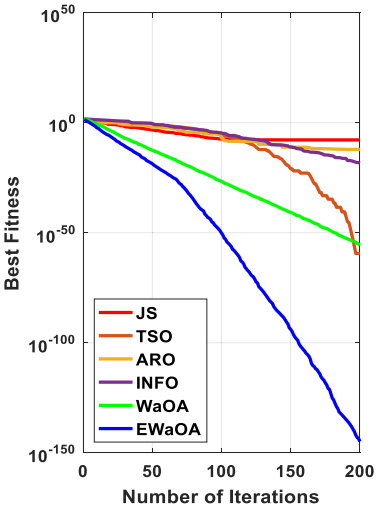

F4

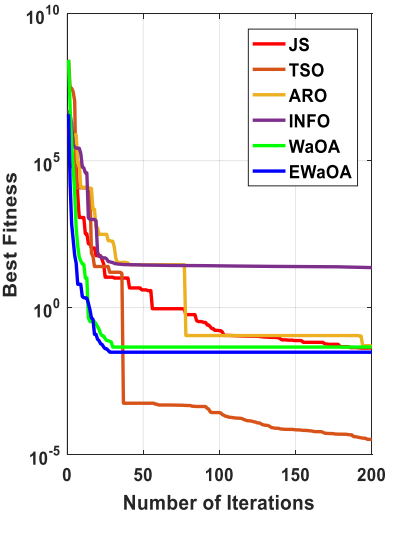

F5

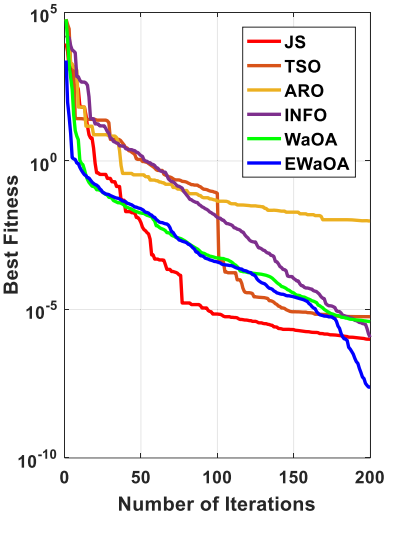

F6

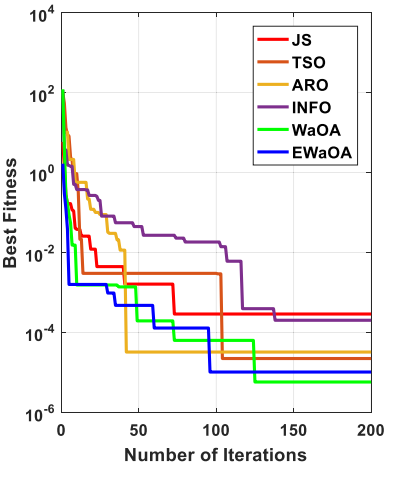

F7

(caption on next page)

Fig. 5. The convergence curves for all methods across the seven benchmark functions.

=0.5 as a constant, where $\overrightarrow{R_B}$ is a vector of uniformly distributed random values ranging from 0 to 1. This scenario occurs during the initial third of iterations when the step size is large, representing a heightened level of exploratory capability. t and T_{max} refer to the current iteration and the maximum iteration, respectively. The most fit solution (E) is chosen to construct a matrix, as illustrated in Eq. (43):

$$E = \begin{bmatrix} x^t_{best\_1.1} & \cdots & x^t_{best\_1.D} \\ \vdots & \ddots & \vdots \\ x^t_{best\_n.1} & \cdots & x^t_{best\_n.D} \end{bmatrix} \tag{43}$$

The matrix E is formed by duplicating the optimal solution n times, where n denotes the count of search agents, and D signifies the number of dimensions. The recommended approach involves employing Lévy flight during the second phase, occurring towards the conclusion of the optimization procedure and characterized through a heightened exploitation capacity. Eqs. (44.1 to 44.3) offer a mathematical depiction of this phase:

$$t > \frac{1}{3}T_{max} \tag{44.1}$$

$$S = \overrightarrow{R_L} \otimes \left(\overrightarrow{R_L} \otimes E - x_i(t)\right) \tag{44.2}$$

$$x_i(t+1) = E + P.CF \otimes S \tag{44.3}$$

The EWaOA algorithm integrates the Lévy method, where R_L is multiplied by E and added to the position to update its location. The Lévy flights enhance the exploration capabilities of algorithms by allowing for larger and more varied search jumps. This strategic incorporation not only facilitates an enhanced exploration capability but also amplifies the likelihood of evading local optima and improves the chances of finding a global optimum. Consequently, these adaptations fortify the algorithm's capacity to explore a broader solution space, thus refining its overall effectiveness. The flowchart of the proposed EWaOA algorithm is depicted in Fig. 4

5. Evaluation and discussion of EWaOA results

5.1. Benchmark functions test

Thorough testing was carried out in consistent settings to establish fair comparison conditions and ensure an objective evaluation. Fifty search agents were deployed for our evaluation, with a 200-iteration limit. Each method has been running 20 times on our own, recognizing that these algorithms are inherently stochastic. MATLAB R2016a software was utilized to implement the algorithms on a high-end Windows 10 64-bit Professional PC through 8 GB of RAM. This made the computing environment for our experiments dependable and consistent. It is noted in this assessment how parameter configurations affected algorithm performance. The parameter values were taken from the original papers written by the creators of each method in order to ensure an even comparison. This approach preserved consistency and got rid of the chance of bias from randomly selected parameters. Especially, jellyfish optimization algorithm (JS) [56], weighted mean of vectors (INFO) [57], artificial rabbits optimization (ARO) [58], tuna swarm optimization (TSO) [59], and the original WaOA were among the algorithms we compared. The EWaOA technique outperformed the other seven benchmark functions, making it stand out [60]. The results consistently beat the results of several modern algorithms, as Table 1 shows. Over a broad range of benchmark functions, EWaOA regularly scored top ranks in terms of worst, average, median, and best outcomes. The EWaOA algorithm excels in consistently discovering optimum outcomes, as shown by its repeated top-ranking performance across various benchmark functions. Its remarkable efficacy in comparison to fashionable techniques underscores its adeptness in tackling demanding optimization challenges. These outcomes substantiate the EWaOA technique as a dependable and robust method for addressing an extensive array of optimization problems.

Fig. 5 illustrates the convergence curves for each method across the 7 benchmark functions (F1, F2, F3, F4, F5, F6, and F7). Applying this visual representation to certain benchmark functions offers insightful information on how each algorithm evolves over iterations. In addition, Fig. 6 displays several boxplots that provide a concise summary of each algorithm's performance over the same set of benchmark functions. The best, average, and worst results of each technique are displayed in these boxplots, providing a thorough overview of their performance. It is noteworthy that the EWaOA technique has remarkable convergence behavior, as shown in Fig. 5, constantly convergent towards optimal solutions for all benchmark functions. To further highlight EWaOA's competitive edge over other algorithms, Fig. 6's boxplots constantly show it as a top-performing algorithm. These convergence curves and boxplot results demonstrate how reliable and efficient the EWaOA method is, as well as how well it performs in reaching convergence and making good results for a variety of benchmark functions.

Furthermore, The Wilcoxon's rank and Friedman's rank tests are performed to validate the superiority of the proposed algorithm as follows:

A. Wilcoxon's rank test results

In this subsection, the variances between EWaOA and other techniques are additional analyzed statistically using the Wilcoxon

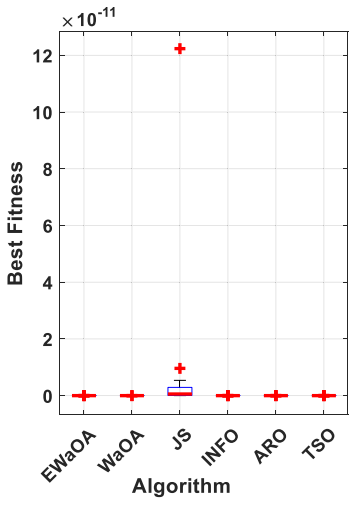

F1

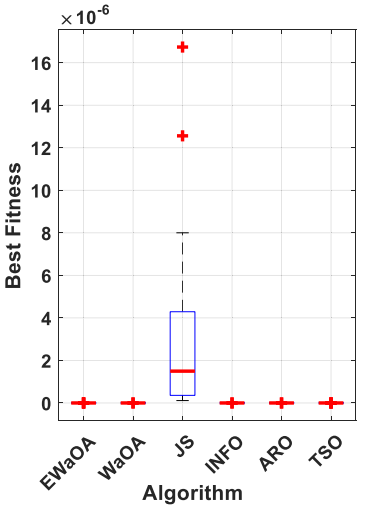

F2

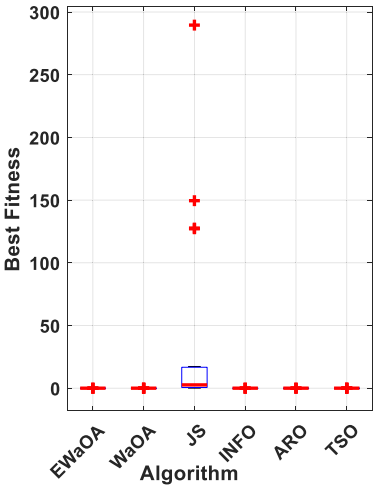

F3

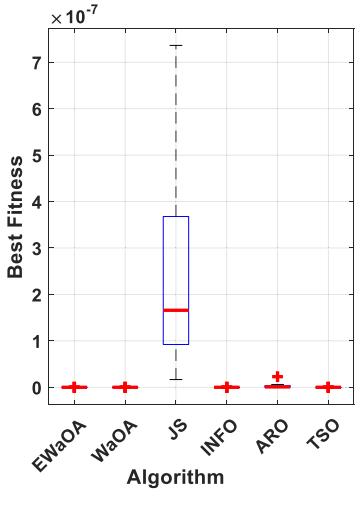

F4

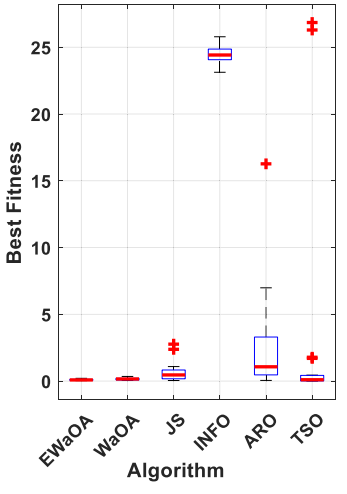

F5

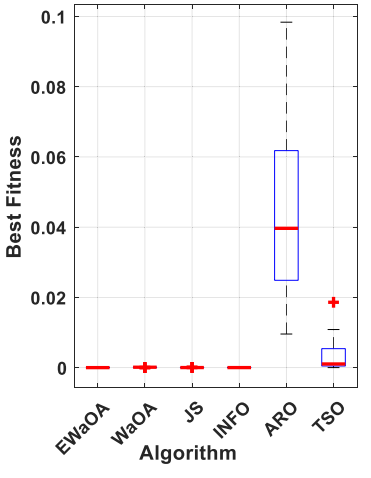

F6

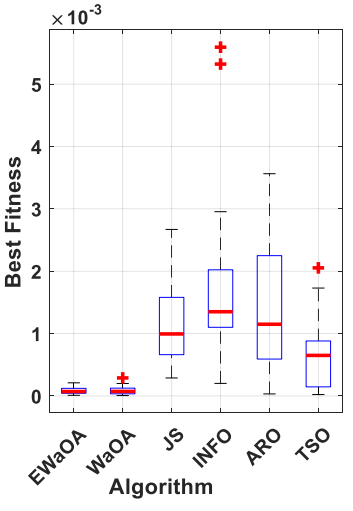

F7

(caption on next page)

Fig. 6. The boxplots representing all techniques for the seven benchmark functions.

rank-sum test (WRST), which is a paired valuation is employed to notice important differences between the two algorithms. The achieved results of the test between EWaOA and each approach, conducted at a significance level ofα=0.05 are presented in Table 2, where the symbols "+/=/-" present whether EWaOA performs better, similarly, or worse than the compared method. Moreover, the table contains statistical findings for EWaOA across different dimensions and functions, demonstrating whether EWaOA performs better, similarly, or worse than the comparison technique. EWaOA verifies superior statistical performance in F1-F7 with Dim=30 when compared to other methods, confirming its important supremacy across most functions. Also, it is confidently concluded that the proposed EWaOA algorithm shows the best overall performance when compared to other techniques.

B. Friedman's rank test results

Table 3 presents the statistical results attained using Friedman tests for seven benchmark functions using the studied methods. A lower ranking value shows superior algorithm performance. Regarding to the results, the ranking order of the six methods is as follows: EWaOA, WaOA, TSO, INFO, JS, and ARO.

5.2. Application of the proposed EWaOA for reliability and security enhancement

In this section, we implement the proposed EWaOA to address the examined problem concerning LORIs, CORIs, and the security index on the IEEE 33-bus EDS, featuring a capacity of 3715 kW & 2300 kVAr. Utilizing the standard IEEE 33-bus EDS, depicted in Fig. 7, we conduct tests and assess the proposed methodology. The number of clients at each service bus is detailed in [32]. The EDS's feeders are categorized into one main residential feeder and three commercial and industrial lateral feeders, delineated as follows:

(i) The main residential feeder is outfitted with a self-closing circuit breaker and 16 sectionalizes at the onset of each branch
(ii) 7 fuses fixed at the outset of every EDS's branch for each commercial lateral feeder.
(iii) A single industrial feeder comprises eight fuses, with one positioned at the start of each branch along the feeder.

The primary objective of this research is to improve multiple reliability indices, encompassing LORIs, CORIs, and the security index of the analyzed EDS, by integrating optimized WTDGs and SMESs. This enhancement is explored through the following scenarios:

***Base case*:** In this case, estimation of the EDS's reliability and security before integration of WTDGs and SMESs.

Case #1: Estimation of the EDS's reliability and security after optimal sites and ratings of WTDGs and SMESs simultaneously without enabled DSTATCOM functionality.

Case #2: Estimation of the EDS's reliability and security in the MOF with optimal weighting factors after optimal sites and ratings of WTDGs and SMESs simultaneously associated with their DSTATCOM functionality.

Case #3: Estimation of the EDS's reliability and security in the MOF without optimal weighting factors (i.e., equal factors) after optimal sites and ratings of WTDGs and SMESs simultaneously associated with their DSTATCOM functionality.

In the current paper, the subsequent presumptions are taken into consideration as shown in Table 4 as follows:

5.2.1. Identifying LSF measures for mixed load

At this juncture, Fig. 8 illustrates the LSF results of the addressed EDS for the mixed load model. Notably, the load points exhibiting the highest LSF values for the mixed load demand model (# 6, 8, 28, 9, 13, 10, 29, 31, 30, 27, 14, 7, 17, 12, 26, 15, 16, 11, 32, 18, and 33) are identified as suitable locations for deploying WTDGs and SMESs.

5.2.2. Verification of the efficiency of the E-WaOA technique

A statistical analysis was conducted to assess the effectiveness of the proposed EWaOA algorithm by comparing its results with those obtained using the WaOA, genetic algorithm (GA), and particle swarm optimization (PSO) techniques. Tables 5 and 6 presents the evaluation of the proposed EWaOA in comparison among the existing algorithms through various statistical metrics, including the best, worst, average, and standard deviation values on using Case #1 and Case #2, respectively. The EWaOA algorithm demonstrated superior statistical performance, evidenced by its lower values in comparison to the conventional WaOA, GA, and PSO techniques. Moreover, the EWaOA offers additional benefits in improving the reliability and security of distribution systems using WTDGs and SMESs.

5.2.3. Optimal sites and ratings of WTDGs & SMESs

This sub-section presents the outcomes related to optimal sites and ratings of WTDGs and SMESs simultaneously in the tested EDS as depicted in Table 7 for Case #1 and Case #2.

5.2.4. Optimum weighting factors

Table 8 displays the optimum weighting factors related to the addressed MOF. It is clearly observed that the index μ_5 related to the EDS's security has a significant weighting factor when it comes to power-quality characteristics for preventing perturbation and congestion in the tested EDN.

Table 2
Statistical results of the Wilcoxon rank-sum test.

EWaOA vs	WaOA		JS		INFO		ARO		TSO	
Function	P	winner	P	winner	P	winner	P	winner	P	winner
F1	6.80E-08	+	6.80E-08	+	6.80E-08	+	6.80E-08	+	6.80E-08	+
F2	6.80E-08	+	6.80E-08	+	6.80E-08	+	6.80E-08	+	6.80E-08	+
F3	6.80E-08	+	6.80E-08	+	6.80E-08	+	6.80E-08	+	6.80E-08	+
F4	6.80E-08	+	6.80E-08	+	6.80E-08	+	6.80E-08	+	6.80E-08	+
F5	2.94E-02	+	2.47E-04	+	6.80E-08	+	9.13E-07	+	8.60E-01	=
F6	6.80E-08	+	6.80E-08	+	6.80E-08	+	6.80E-08	+	6.80E-08	+
F7	7.15E-01	=	6.80E-08	+	7.90E-08	+	1.20E-06	+	1.04E-04	+
WRST (+/=/-)	6/1/0		7/0/0		7/0/0		7/0/0		6/1/0	

Table 3
Friedman test for the six algorithms.

Function	EWaOA	WaOA	JS	INFO	ARO	TSO
F1	1	2.1	6	4	5	2.9
F2	1	2.05	6	4	5	2.95
F3	1	3	6	4	5	2
F4	1	2.1	5.95	4	5.05	2.9
F5	1.95	2.65	3.45	5.9	4.5	2.55
F6	1	3.95	2.6	2.55	6	4.9
F7	1.6	1.75	4.6	4.95	4.45	3.65
Mean ranks	1.221429	2.514286	4.942857	4.2	5	3.121429

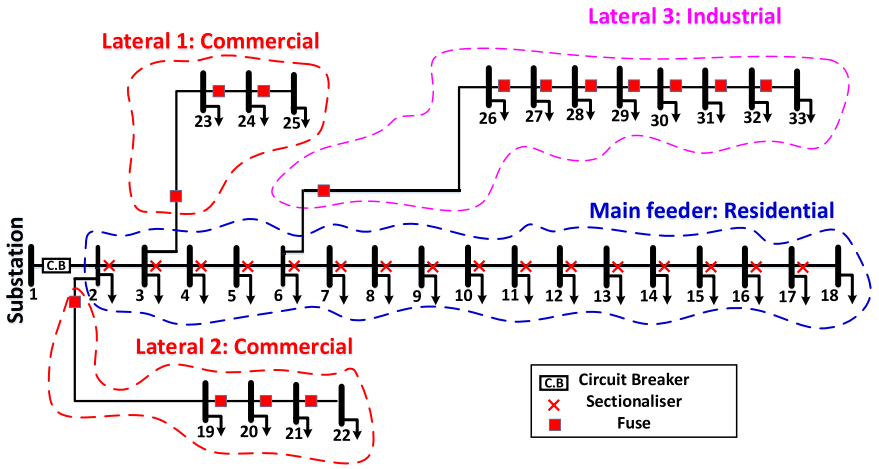

Fig. 7. The schematic diagram of the typical IEEE 33-bus EDS.

5.2.5. Enhancement of the LORIs

The daily LORIs, which includes the ENS and AENS, are computed as composite values derived from the hourly LORIs. Table 9 presents the ENS and AENS values for a full day before and after the incorporation of WTDGs and SMESs, both without and with their DSTATCOM functionality (Case #1 and Case #2, respectively). This is an addition to the results of the ENS and AENS are depicted on using Case #3. It is evident that the introduction of WTDGs and SMESs results in a reduction of the daily ENS and AENS, with decreases of 5.32 % in Case #1, 7.72 % in Case #2, and 7.65 % in Case #3 compared to the base-case scenario. Consequently, there is an enhancement in ENS and AENS for each respective case. It is obvious that the best results for the ENS and their average are the results of Case #2, which it's MOF depending on optimal weighting factors. Furthermore, the AENS values for each hour following the simultaneous integration of WTDGs and SMESs are lower than those before their integration in the studied EDS, indicating an enhancement in the EDS's LORIs, as depicted in Fig. 9.

5.2.6. Improvement of the CORIs

Table 10 provides an assessment of the daily SAIDI (h/Cust. /yr.), CAIDI (h/Cust. /inter.), SAIFI (inter./Cust. /yr.), and ASUI with and without the deployment of WTDGs and SMESs, both without and with their DSTATCOM functionality (Case #1 and Case #2, respectively). This is an addition to the results of the CORIs are depicted on using Case #3. It is evident that employing WTDGs and

Table 4
Basic assumptions for different components of the investigated EDS.

Component	Assumptions
SMES unit	– It discharges when the load exceeds 75 % of the peak load. – It charges using surplus energy generated by WTDGs. – The rated power of the SMESs ranges from 0 to 1.1 MW. – The rated capacity of the SMESs ranges from 0 to 5 MWh. – The charging and discharging efficiency of SMESs is set at 0.98.
EDS	– Two load nodes within the EDS are designated for the installation of one WTDG and one SMES each. – The λ_i^{init} for feeder branch is set at 0.2 failures per kilometer per year. – Circuit breakers, sectionalizes, fuses, and system buses are assumed to have complete reliability. – For the i^{th} feeder, λ_i^{best} is determined as 85 % of the initial rate λ_i^{init} – The switching time for feeder branch is set at 0.5 h. – The repair time for feeder branch is 4 h for a branch in the primary feeder and 2 h for a branch in the lateral feeders.
WTDG unit	– The maximum power per load point is 2.2 MW.

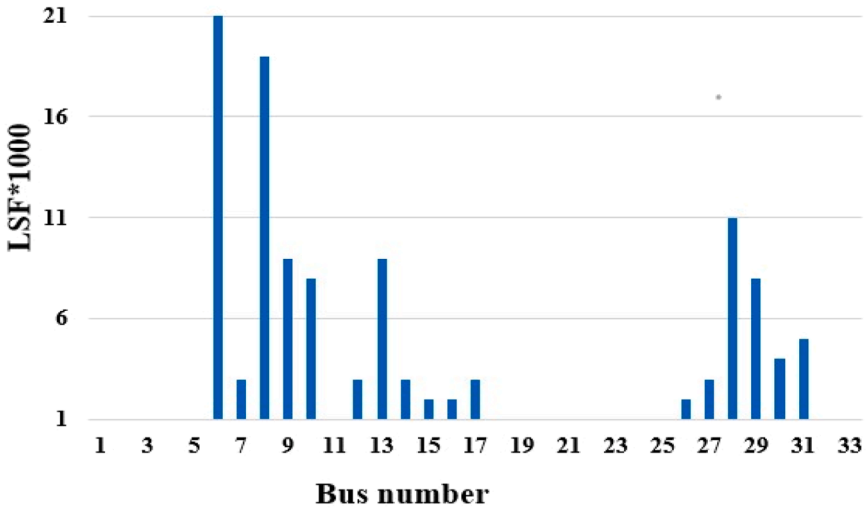

Fig. 8. Outcomes of the values of the LSF for mixed load model.

SMESs along with their DSTATCOM functionality (Case #2) leads to a reduction in the daily SAIFI, SAIDI, CAIDI, and ASUI by 7.01 %, 8.03 %, 1.21 %, and 7.91 %, respectively, compared to Case #1 and Case #3. Consequently, there is an improvement in the values of CORIs on using Case #2, which it's MOF depending on optimal weighting factors. Additionally, Figs. 10, 11, 12, and 13 illustrate that the different types of CORIs during each hour over the day after the implementation of WTDGs and SMESs with their DSTATCOM functionality are lower than those before their integration in the studied EDS, indicating an enhancement in the EDS's CORIs.

5.2.7. Improvement of the security index

A comparison of NSI values for the previous case studies is depicted in Table 11. It is shown that the deployment of WTDGs and SMESs results in a reduction of the daily NSI by 25.85 % in Case #1, 37.23 % in Case #2, and 36.98 % in Case #3 compared to the base-case scenario. Therefore, there is an improvement in the NSI value on using Case #2, which it's MOF depending on optimal weighting factors. Additionally, the hourly NSI values following the simultaneous integration of WTDGs and SMESs are lower than those before their integration in the studied EDS, indicating an enhancement in the EDS's security, as shown in Fig. 14. This improvement can be attributed to the decrease in grid current-flow magnitude within the EDS due to the deployment of WTDGs and SMESs.

5.2.8. Examination of SMES's SOC

The first SMES's charging and discharging powers occur during hours (15–18) and (20–21), respectively, with SOC_{ini1} equal to 0.44, as depicted in Fig. 15(a). Also, the second SMES's charging and discharging powers occurred during hours (15–18) and (20–21), respectively, with SOC_{ini2} equal to 0.36 for the mixed load under consideration, as depicted in Fig. 15(b).

Table 5
Statistical results of the EWaOA in comparison among the existing algorithms on using Case #1.

Parameter	Type of optimizer			
	EWaOA	WaOA	GA	PSO
Best	**0.830380**	0.833819	0.846447	0.837794
Worst	**0.897435**	1000.578	1000.79	1000.927
Average	**0.853645**	34.17862	434.0898	267.4951
STD	**0.018392**	182.5237	503.8749	449.7325

Table 6
Statistical results of the EWaOA in comparison among the existing algorithms on using Case #2.

Parameter	Type of optimizer			
	EWaOA	WaOA	GA	PSO
Best	**0.747377**	0.760629	0.78337	0.7624
Worst	**0.759453**	0.776178	1.069076	0.8050
Average	**0.753541**	0.768443	0.834051	0.7777
STD	**0.002816**	0.004042	0.057293	0.0097

Table 7
Optimal sites and ratings of WTDGs & SMESs.

Items	1st WTDG (KW /# Load point)	1st SMES (KW/ KWh)	2nd WTDG (KW /# Load point)	2nd SMES (KW/ KWh)
Data	2200 / # 6	584/2705	645 / # 14	337/1289

Table 8
The optimum weighting factors related to the studied MOF.

Item	weighting factors				
	μ_1	μ_2	μ_3	μ_4	μ_5
Value	0.1	0.1	0.1	0.1	0.6

5.2.9. Examination of reactive power injected by WTDGs& SMESs

Fig. 16 illustrates the optimal delivered/consumed reactive powers by the connected inverters of the WTDGs and SMESs, considering their DSTATCOM functionality. It is evident that positive reactive power indicates injection, while negative indicates absorption. These quantities of delivered/consumed reactive powers have notable impacts on the LORIs, CORIs, and security index of the tested EDS.

5.3. Final discussion of this study

The proposed EWaOA outperforms the other algorithms considered (i.e., WaOA, JS, INFO, ARO, and TSO) based on the results of benchmark function tests, Wilcoxon's rank test, and Friedman's rank test. Additionally, the EWaOA demonstrates superior performance in solving the problem related to LORIs, CORIs, and the security index for the IEEE 33-bus EDS. Moreover, the optimal indices for LORIs, CORIs, and the security index are obtained in Case #2, which evaluates the reliability and security of the EDS within the MOF using optimal weighting factors, after determining the optimum sites and ratings for WTDGs and SMESs, along with their DSTATCOM functionality are the best.

6. Conclusions

In this research, an effective algorithm, EWaOA, has been presented to address global optimization challenges while simultaneously enhancing the reliability and security of electrical distribution systems (EDS). Through rigorous evaluation on seven benchmark functions, the performance of the intended EWaOA technique was assessed, comparing its outcomes with those of the

Table 9
Values of the LORIs for various studied cases.

Items	Base case	Case #1	Case #2	Case #3
ENS (MWh/yr)	582.38	551.35	537.40	537.81
AENS (kWh/Cust./yr)	31.99	30.2937	29.5277	29.5502
ENS and *AENS* reduction %		5.32	**7.72**	7.65

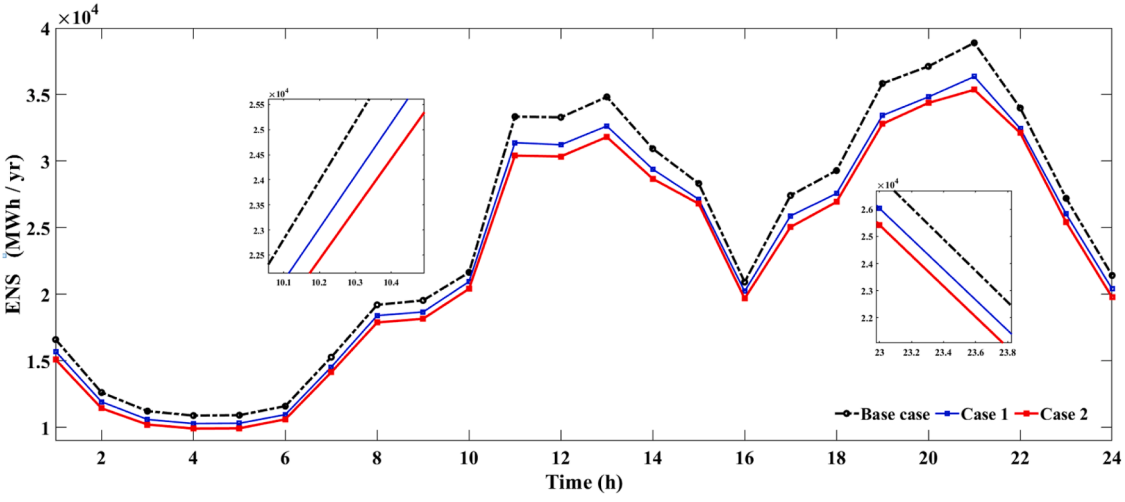

(a)

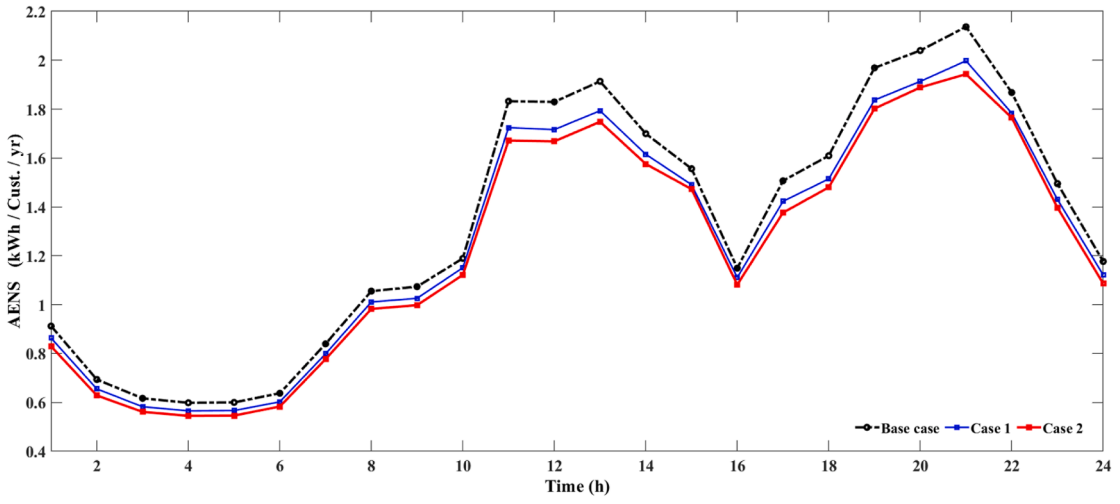

(b)

Fig. 9. Hourly values of the (a) ENS and (b) AENS for different case studies.

Table 10
Values of the CORIs for various studied cases.

Items	Base case	Case #1	Case #2	Case #3
SAIFI	177.32	168.6438	164.8864	164.8894
***SAIFI* reduction %**		4.91	**7.01**	7.0102
SAIDI	298.98	282.9986	274.9783	275.0934
***SAIDI* reduction %**		5.35	**8.03**	7.989
CAIDI	40.46	40.2684	39.9733	39.9773
***CAIDI* reduction %**		0.49	**1.211**	1.193
ASUI	0.0341	0.0323	0.0314	0.0314
***ASUI* reduction %**		5.27	**7.91**	7.91

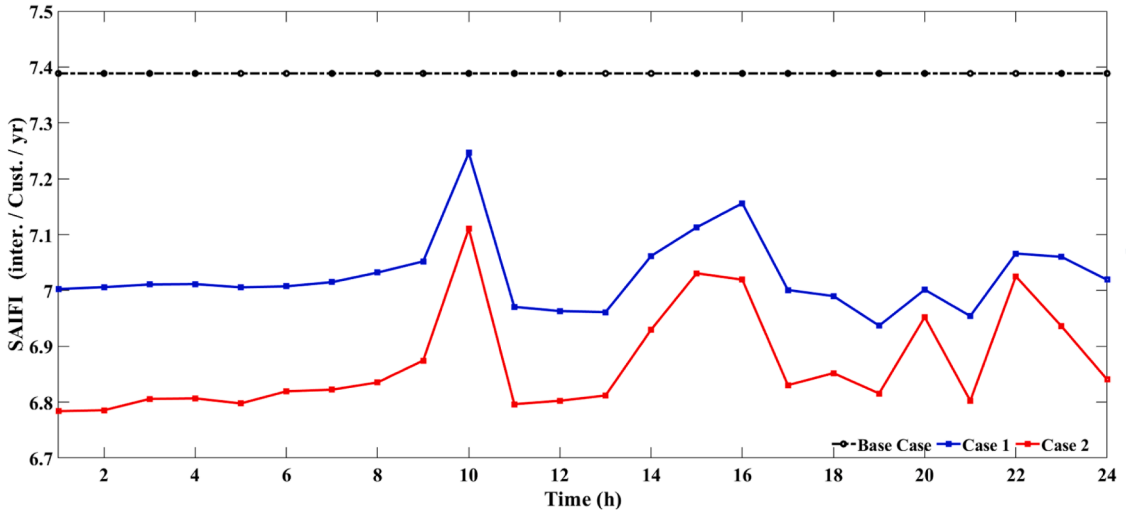

Fig. 10. Hourly values of the SAIFI for the above-mentioned case studies.

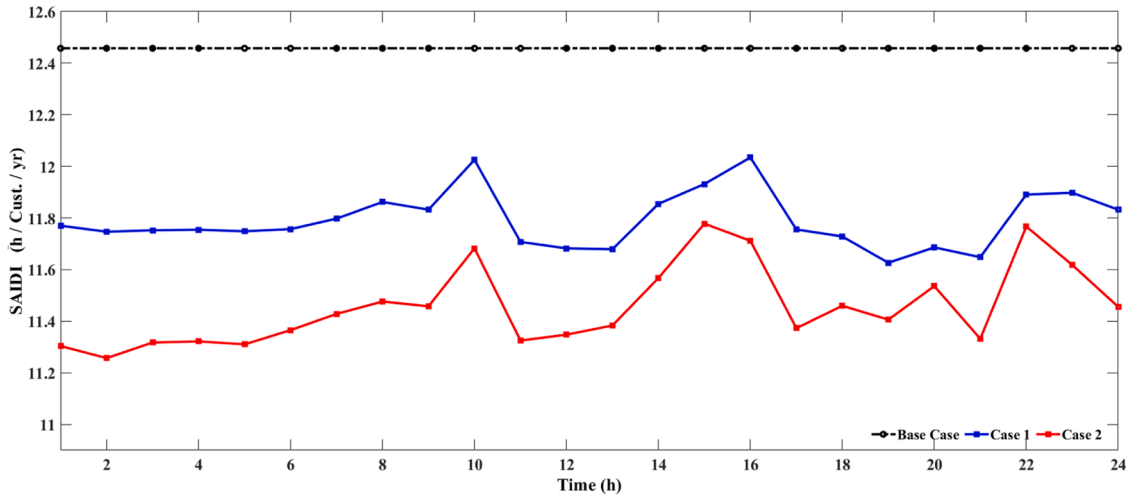

Fig. 11. Hourly values of the SAIDI for the above-mentioned case studies.

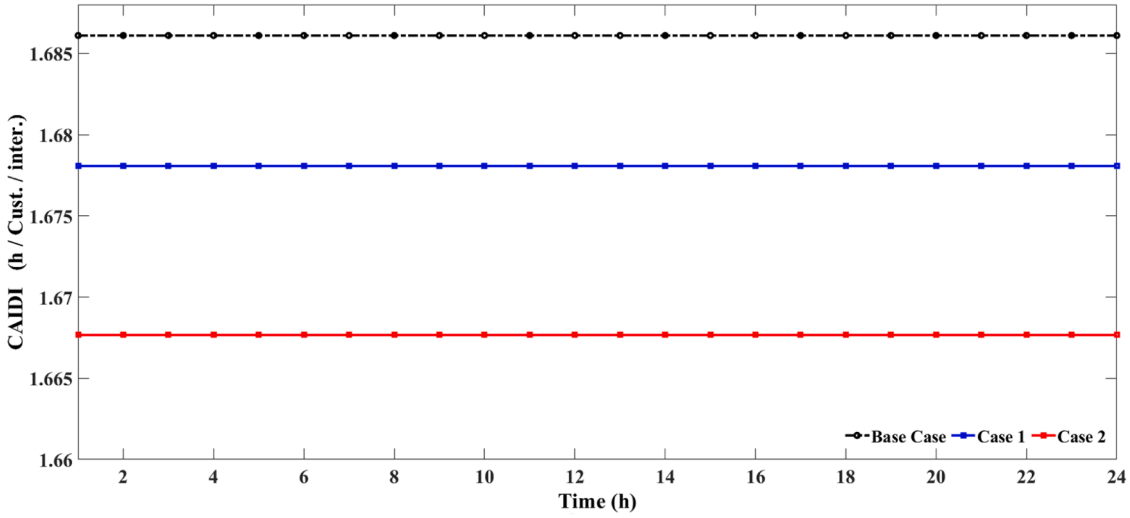

Fig. 12. Hourly values of the CAIDI for the above-mentioned case studies.

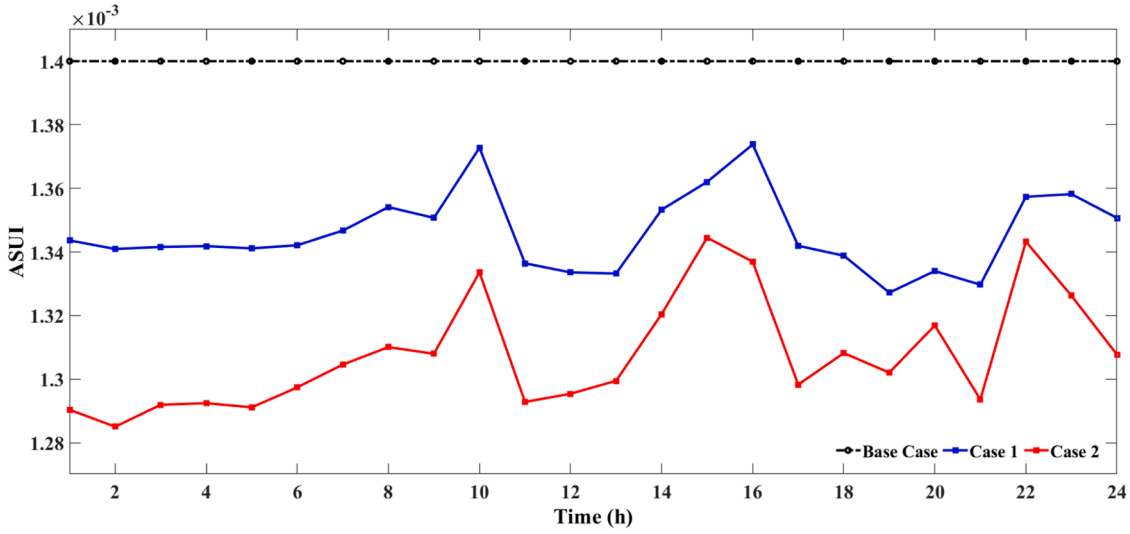

Fig. 13. Hourly values of the ASUI for the above-mentioned case studies.

Table 11
Values of the NSIs for various studied cases.

Items	Base case	Case #1	Case #2	Case #3
NSI	205.38	152.2730	128.9021	129.6020
NSI reduction %		25.85	**37.23**	36.98

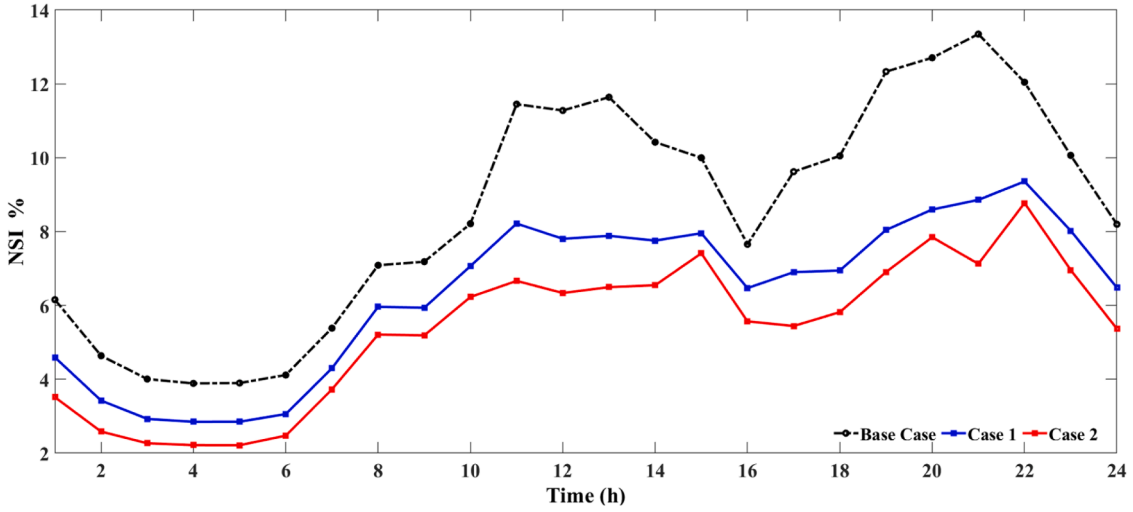

Fig. 14. Per-hour *NSI* outcomes for different case studies.

original WaOA algorithm and other contemporary algorithms across various functions. Several key conclusions emerged:

An approach for optimizing the siting and ratings of WTDGs and SMESs has been proposed, considering their DSTATCOM functionality, with the aim of improving the security and reliability of EDS. This involved the simultaneous minimization of key reliability indices such as NSI, SAIFI, ASUI, SAIDI, and ENS using a Multi-Objective Optimization Framework (MOF) with optimized weight factors. Employing the LSF to identify the most suitable EDS buses for the inclusion of WTDGs and SMESs enhances the efficiency and effectiveness of the deployment process. Investigation into the optimum discharge and charge and powers of SMESs, along with their initially SOC, was conducted, along with examining the impact of the FFR mechanism and the setting up of protection devices on the EDS's reliability, providing insights into their role in enhancing the system's reliability.

Comprehensive testing of the proposed method was carried out on the IEEE 33-bus EDS, utilizing a mixed TVVD load model to simulate real-world conditions. The outcomes show that the optimal integration of WTDGs and SMESs, along with their DSTATCOM functionality, can significantly enhance the EDS's reliability and security, leading to notable improvements in system performance. Overall, this research highlights the capability of the intended EWaOA algorithm to address global optimization challenges while concurrently improving the reliability and security of EDS.

The investigated IEEE 33-bus EDN is a small-scale network, which may be a technical limitation of the present research work. However, the economic limitation of the SMES is its high cost. But, its implementation of suitable high-temperature superconductors (HTS) can face this challenge. With the use of the HTS system, the refrigeration cost is minimized and the system is improved and stable by producing lower mechanical stresses. These limitations along with the PV's installation and the weather uncertainties will be considered in future research work.

CRediT authorship contribution statement

Mohamed Khamies: Conceptualization, Methodology, Software, Data curation, Resources, Writing – original draft, Visualization, Investigation, Validation. **Mohamed Hashem:** Conceptualization, Methodology, Software, Data curation, Resources, Formal analysis, Visualization, Investigation, Validation, Writing – review & editing. **Salah Kamel:** Conceptualization, Visualization, Software, Investigation, Supervision, Validation, Writing – review & editing. **Mohamed H. Hassan:** Conceptualization, Methodology, Investigation, Validation. **Abdelfatah Ali:** Conceptualization, Visualization, Software, Investigation, Supervision, Validation, Writing – review & editing.

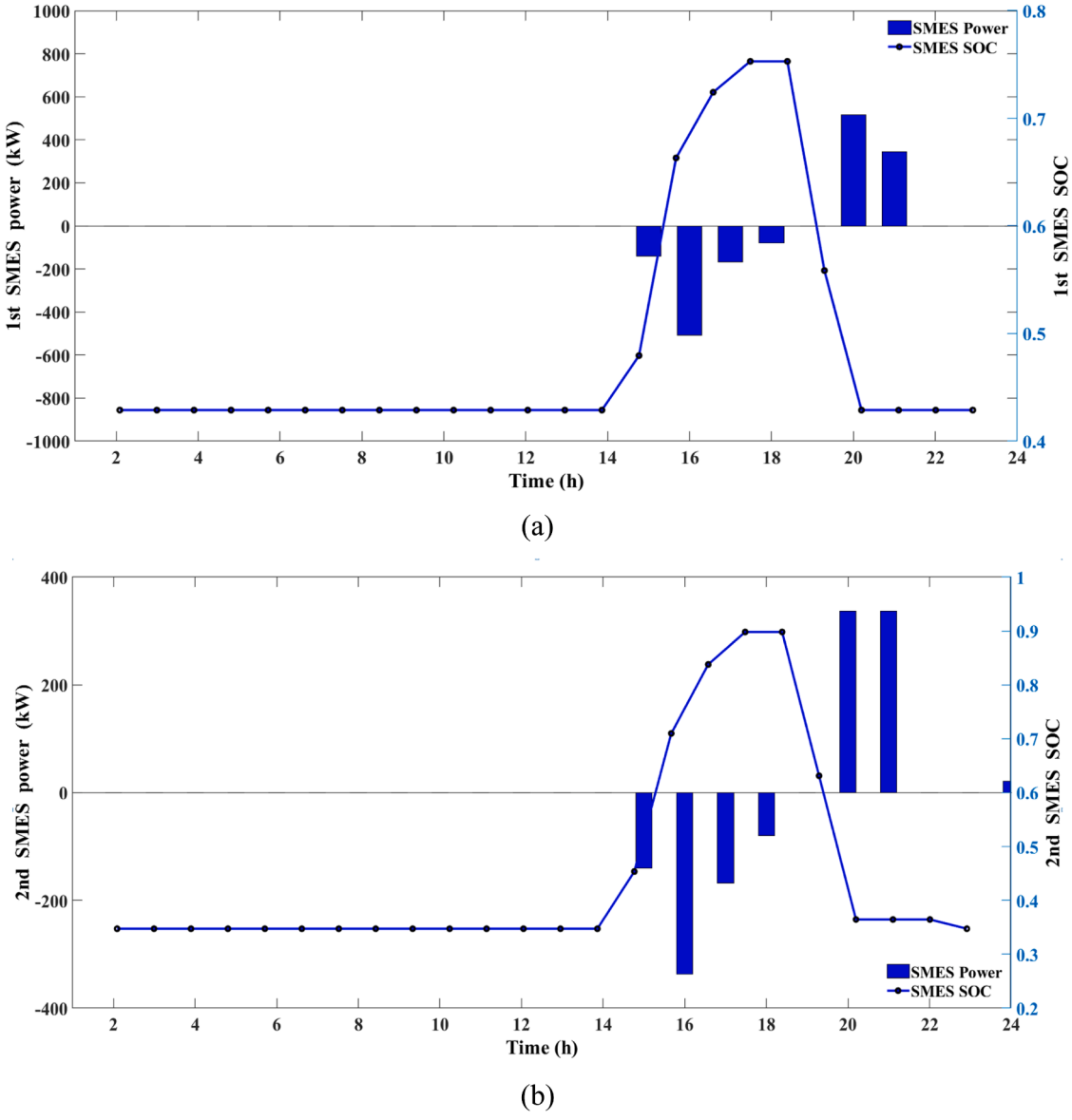

Fig. 15. Hourly SOC and interchange powers of (a) 1st SMES and (b) 2nd SMES.

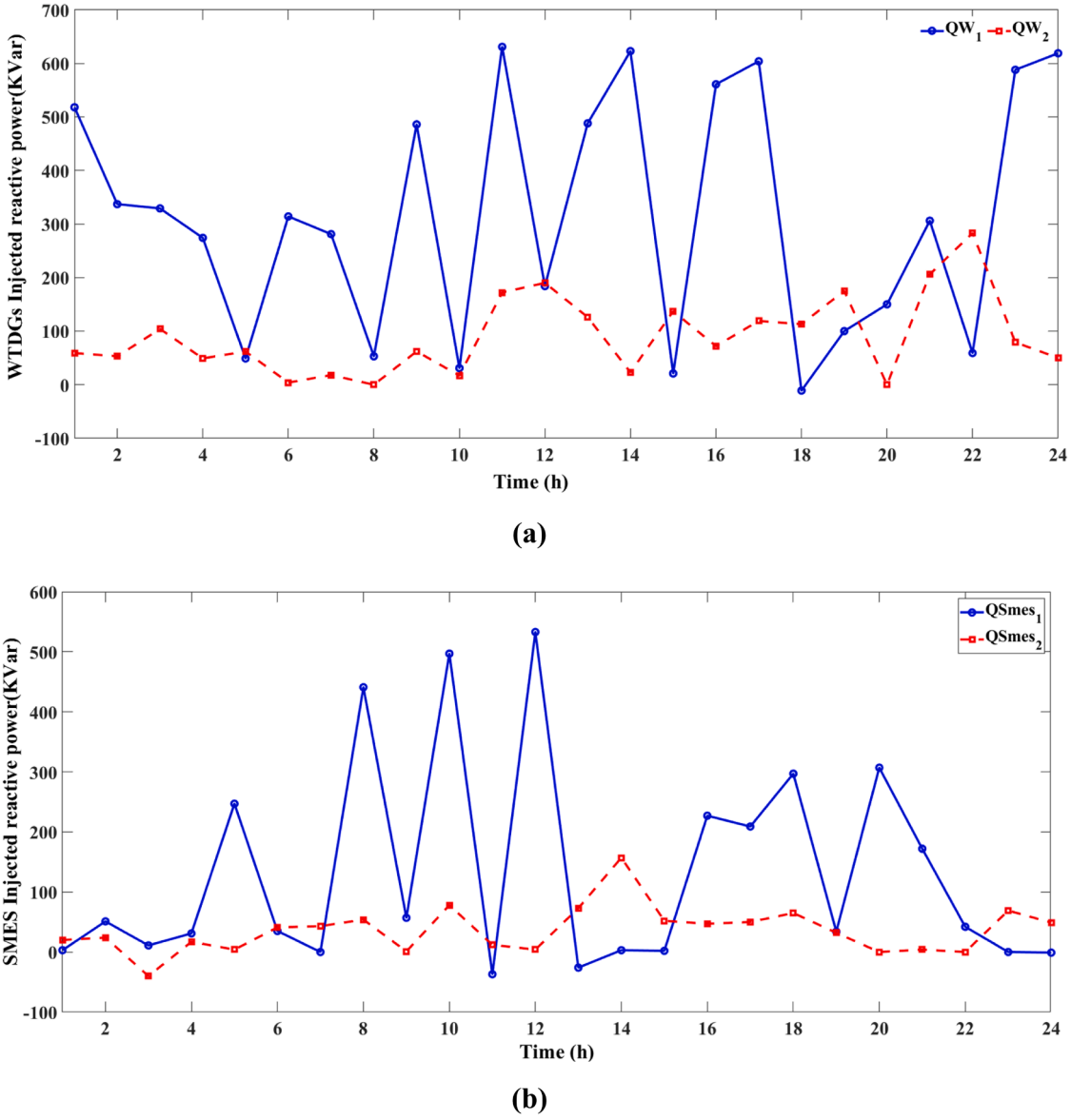

Fig. 16. Optimal delivered/consumed reactive powers by the connected inverters of the (a) WTDGS and (b) SMESs.

Declaration of competing interest

The authors declare that they have no known competing financial interests or personal relationships that could have appeared to influence the work reported in this paper. The authors declare the following financial interests/personal relationships which may be considered as potential competing interests: The authors declare that they have no known competing financial interests or personal relationships that could have appeared to influence the work reported in this paper.

Data availability

Data will be made available on request.

References

[1] Wang X, Li Z, Shahidehpour M, Jiang C. Robust line hardening strategies for improving the resilience of distribution systems with variable renewable resources. IEEE Trans Sustain Energy 2017;10:386–95.

[2] Ali A, Mahmoud K, Lehtonen M. Optimization of photovoltaic and wind generation systems for autonomous microgrids with PEV-parking lots. IEEE Syst J 2021; 16:3260–71.
[3] Lara JD, Olivares DE, Canizares CA. Robust energy management of isolated microgrids. IEEE Syst J 2018;13:680–91.
[4] Du Y, Wu J, Li S, Long C, Onori S. Coordinated energy dispatch of autonomous microgrids with distributed MPC optimization. IEEE Trans Ind Inform 2019;15: 5289–98.
[5] Xu D, Zhou B, Wu Q, Chung CY, Li C, Huang S, Chen S. Integrated modelling and enhanced utilization of power-to-ammonia for high renewable penetrated multi-energy systems. IEEE Trans Power Syst 2020;35:4769–80.
[6] Ali A, Mahmoud K, Lehtonen M. Multiobjective photovoltaic sizing with diverse inverter control schemes in distribution systems hosting EVs. IEEE Trans Ind Inform 2020;17:5982–92.
[7] Shi L, Wang C, Liu S, Cheng X, Liu Q, Zhuge W, Zhang Y. Energy optimization and economic study of an energy storage system based on a carbon dioxide-to-methanol process. J Energy Storage. 2023;62:106846.
[8] Chen H, Wu H, Kan T, Zhang J, Li H. Low-carbon economic dispatch of integrated energy system containing electric hydrogen production based on VMD-GRU short-term wind power prediction. Int J Electr Power Energy Syst 2023;154:109420.
[9] Argyrou MC, Christodoulides P, Kalogirou SA. Energy storage for electricity generation and related processes: technologies appraisal and grid scale applications. Renew Sustain Energy Rev 2018;94:804–21.
[10] Afzali P, Keynia F, Rashidinejad M. A new model for reliability-centered maintenance prioritisation of distribution feeders. Energy 2019;171:701–9.
[11] Rahmani-andebili M. Simultaneous placement of DG and capacitor in distribution network. Electr Power Syst Res 2016;131:1–10.
[12] Abdel-Salam M, Elnozahy A, Elgamal M. Minimum power loss based design of SMES as influenced by coil material. J Energy Storage 2020;30:101461.
[13] Hannan MA, Hoque MM, Mohamed A, Ayob A. Review of energy storage systems for electric vehicle applications: issues and challenges. Renew Sustain Energy Rev 2017;69:771–89.
[14] Elshiekh M, Elwakeel A, Venuturumilli S, Alafnan H, Pei X, Zhang M, Yuan W. Utilising SMES-FCL to improve the transient behaviour of a doubly fed induction generator DC wind system. Int J Electr Power Energy Syst 2021;131:107099.
[15] V.S.V. G, S. Madichetty, Application of superconducting magnetic energy storage in electrical power and energy systems: a review, (2018) 358–68.
[16] Qais MH, Hasanien HM, Alghuwainem S. Output power smoothing of wind power plants using self-tuned controlled SMES units. Electr Power Syst Res 2020; 178:106056.
[17] Hashem M, Abdel-Salam M, Nayel M, Th M. El-Mohandes, mitigation of voltage sag in a distribution system during Start-up of water-pumping motors using superconducting magnetic energy storage: a case study. J Energy Storage 2022;55:105441.
[18] Said Sayed M, Abdel-Salam Mazen, Nayel Mohamed, Hashem Mohamed, Kamel Salah, Jurado Francisco, Ebeed Mohamed. Optimal design and cost of superconducting magnetic energy storage for voltage sag mitigation in a real distribution network. J Energy Storage 2023;73:108864.
[19] Anand MP, Bagen B, Rajapakse A. Probabilistic reliability evaluation of distribution systems considering the spatial and temporal distribution of electric vehicles. Electr Power Energy Syst 2020;117:105609.
[20] Fathy A, Abdelaziz AY. Grey wolf optimizer for optimal sizing and siting of energy storage system in electric distribution network. Electr Power Components Syst 2017;45:601–14.
[21] Lata P, Vadhera S. Reliability Improvement of Radial Distribution System by Optimal Placement and Sizing of Energy Storage System using TLBO. J Energy Storage. 2020;30:101492.
[22] Samantaray S, Kayal P. Capacity assessment and scheduling of batterystorage systems for performance and reliability improvement of solarenergy enhanced distribution systems. J Energy Storage 2023;66:107479.
[23] Kumar S, Sarita K, Vardhan A, Elavarasan R, Saket RK, Das N. Reliability assessment of wind-solar PV integrated distribution system using electrical loss minimization technique. Energies 2020;13:5631.
[24] Hamidan M-A, Borousan F. Optimal planning of distributed generation and battery energy storage systems simultaneously in distributionnetworks for loss reduction and reliability improvement. J Energy Storage 2022;46:103844.
[25] Abdelsalam AA. Optimal distributed energy resources allocation for enriching reliability and economic benefits using sine-cosine algorithm. Tech Econom Smart Grids Sust Energy 2020;8:1–18.
[26] Nowdeh SA, Davoudkhani IF, Moghaddam MJH, Najmi ES. Fuzzy multi-objective placement of renewable energy sources in distribution system with objective of loss reduction and reliability improvement using a novel hybrid method. Appl Soft Comput J 2019;77:761–79.
[27] Jafar-nowdeh A, Babanezhad M, Arabi-nowdeh S. Meta-heuristic matrix moth – flame algorithm for optimal reconfiguration of distribution networks and placement of solar and wind renewable sources considering reliability. Environ Technol Innov 2020;20:101118.
[28] Duan D, Ling X, Wu X, Zhong B. Reconfiguration of distribution network for loss reduction and reliability improvement based on an enhanced genetic algorithm. Int. J Electr Power Energy Syst 2015;64:88–95.
[29] Yin H, Wang Z, Liu Y, Qudaih Y, Tang D, Liu T, et al. Operational reliability assessment of distribution network with energy storage systems. IEEE Syst J 2022;17 (1):629–39.
[30] Abdelsalam AA. Maximizing technical and economical benefits of distribution systems by optimal allocation and hourly scheduling of capacitors and distributed energy resources. Aust J Electr Electron Eng 2019;00:1–13.
[31] Abdelsalam AA, Mansour HSE, Abdelsalam AA, Mansour HSE. Optimal allocation and hourly scheduling of capacitor banks using sine cosine algorithm for maximizing technical and economic benefits. Electr Power Components Syst 2019;0:1–15.
[32] Hashem M, Abdel-salam M, Nayel M, El-mohandes MT. A Bi-level optimizer for reliability and security assessment of a radial distribution system supported by wind turbine generators and superconducting magnetic energy storages. J Energy Storage 2022;51:104356.
[33] Ali A, Mahmoud K, Lehtonen M. Maximizing hosting capacity of uncertain photovoltaics by coordinated management of OLTC, VAr sources and stochastic EVs. Int J Electr Power Energy Syst 2021;127:106627.
[34] Aleem SA, Hussain SS, Ustun TS. A review of strategies to increase PV penetration level in smart grids. Energies 2020;13:636.
[35] Ali A, Mahmoud K, Lehtonen M. Enhancing hosting capacity of intermittent wind turbine systems using bi-level optimisation considering OLTC and electric vehicle charging stations. IET Renew Power Gener 2020;14:3558–67.
[36] Ebeed M, Hashem M, Aly M, Kamel S, Jurado F, Mohamed EA, Abd El Hamid AM. Optimal integrating inverter-based PVs with inherent DSTATCOM functionality for reliability and security improvement at seasonal uncertainty. Sol Energy 2023:112200.
[37] Das CK, Bass O, Kothapalli G, Mahmoud TS, Habibi D. Optimal placement of distributed energy storage systems in distribution networks using artificial bee colony algorithm. Appl Energy 2018;232:212–28.
[38] Das CK, Bass O, Mahmoud TS, Kothapalli G, Mousavi N, Habibi D, et al. Optimal allocation of distributed energy storage systems to improve performance and power quality of distribution networks. Appl Energy 2019;252:113468.
[39] Das CK, Bass O, Mahmoud TS, Kothapalli G, Masoum MAS, Mousavi N. An optimal allocation and sizing strategy of distributed energy storage systems to improve performance of distribution networks. J Energy Storage 2019;26:100847.
[40] Kayal P, Chanda CK. Strategic approach for reinforcement of intermittent renewable energy sources and capacitor bank for sustainable electric power distribution system. Int J Elect Power Energy 2016;83:335–51.
[41] Kamel RM, Hashem M, Ebeed M, Ali A. Enhancing the reliability and security of distribution networks with plug-in electric vehicles and wind turbine generators considering their stochastic natures. Sustain Energy Grids Netw 2024;39:101439.
[42] Hashem M, Abdel-salam M, El-mohandes MT, Nayel M. Optimal placement and sizing of wind turbine generators and superconducting magnetic energy storages in a distribution system. J Energy Storage 2021;38:102497.
[43] Ahmed A, Nadeem MF, Sajjad IA, Bo R, Khan IA, Raza A. Probabilistic generation model for optimal allocation of wind DG in distribution systems with time varying load models. Sustain Energy, Grids Netw 2020;22:100358.

[44] Yarahmadi M, Shakarami MR. An analytical and probabilistic method to determine wind distributed generators penetration for distribution networks based on time-dependent loads. Electr Power Energy Syst 2018;103:404–13.
[45] Hung DQ, Mithulananthan N, Bansal RC. Analytical strategies for renewable distributed generation integration considering energy loss minimization. Appl Energy 2013;105:75–85.
[46] M. Khasanov, A. Al-durra, S. Kamel, C. Rahmann, H.M. Hasanien, Optimal distributed generation and battery energy storage units integration in distribution systems considering power generation uncertainty, (2021) 3400–22.
[47] Mukherjee P, Rao VV. Superconducting magnetic energy storage for stabilizing grid integrated with wind power generation systems. J Mod Power Syst Clean Energy 2019;7:400–11.
[48] Chen Z, Xiao XY, Li CS, Zhang Y, Zheng ZX. Study on unit commitment problem considering large-scale superconducting magnetic energy storage systems. IEEE Trans Appl Supercond 2016;26:5701306.
[49] Kumar S, Sarita K, Vardhan ASS, Elavarasan RM, Saket RK, Das N. Reliability assessment of wind-solar PV integrated distribution system using electrical loss minimization technique. Energies 2020;13:1–30.
[50] Kayal P, Chanda CK. Optimal mix of solar and wind distributed generations considering performance improvement of electrical distribution network. Renew Energy 2015;75:173–86.
[51] Abdelsalam AA, Mansour HSE, Abdelsalam AA, Mansour HSE. Optimal allocation and hourly scheduling of capacitor banks using sine cosine algorithm for maximizing technical and economic benefits. Electr Power Components Syst 2019;0:1–15.
[52] Trojovský P, Dehghani M. A new bio-inspired metaheuristic algorithm for solving optimization problems based on walruses behavior. Sci Rep 2023;13:8775.
[53] Faramarzi A, Heidarinejad M, Mirjalili S, Gandomi AH. Marine Predators Algorithm: a nature-inspired metaheuristic. Expert Syst Appl 2020;152:113377.
[54] Khamies M, Elkasem AHA, Hassan MH, Kamel S. Enhancing frequency stability in diverse power systems with conventional and renewable energy sources based on an innovative LFC and controlled energy storage integration. J Energy Storage 2023;73:108960.
[55] Awad A, Kamel S, Hassan MH, Elnaggar MF. An enhanced tuna swarm algorithm for optimizing FACTS and wind turbine allocation in power systems. Electr Power Components Syst. 2024;52:863–78.
[56] Chou J-S, Truong D-N. A novel metaheuristic optimizer inspired by behavior of jellyfish in ocean. Appl Math Comput 2021;389:125535.
[57] Ahmadianfar I, Heidari AA, Noshadian S, Chen H, Gandomi AH. INFO: an efficient optimization algorithm based on weighted mean of vectors. Expert Syst Appl 2022;195:116516.
[58] Wang L, Cao Q, Zhang Z, Mirjalili S, Zhao W. Artificial rabbits optimization: a new bio-inspired meta-heuristic algorithm for solving engineering optimization problems. Eng Appl Artif Intell 2022;114:105082.
[59] Xie L, Han T, Zhou H, Zhang Z-R, Han B, Tang A. Tuna swarm optimization: a novel swarm based metaheuristic algorithm for global optimization. Comput Intell Neurosci 2021;2021:9210050.
[60] Hassan MH, Kamel S, Jurado F, Ebeed M, Elnaggar MF. Economic load dispatch solution of large-scale power systems using an enhanced beluga whale optimizer. Alexandria Eng J 2023;72:573–91.